 doi:10.20944/preprints201609.0106.v1

Article

New Scientific Contribution on the 2-D Subdomain Technique in Cartesian Coordinates: Taking into Account of Iron Parts

Frédéric Dubas [1,*] and Kamel Boughrara [2]

[1] ENERGY Department, FEMTO-ST Institute, UMR CNRS 6174, UBFC, Belfort, France; FDubas@gmail.com
[2] Laboratoire de Rcherche en Electrotechnique (LRE-ENP), Algiers, 10 av. Pasteur, El Harrach, BP 182, 16200, Algeria; kamel.boughrara@g.enp.edu.dz
* Correspondence: FDubas@gmail.com; Tel.: +3-338-457-8203

Abstract: The most significant assumptions in the subdomain technique (i.e., based on the formal resolution of Maxwell's equations applied in subdomain) is defined by: *"The iron parts (i.e., the teeth and the back-iron) are considered to be infinitely permeable, i.e.,* $\mu_{iron} \rightarrow +\infty$*, so that the saturation effect is neglected"*. In this paper, the author presents a new scientific contribution on improving of this method in two-dimensional (2-D) and in Cartesian coordinates by focusing on the consideration of iron. The subdomains connection is carried out in the two directions (i.e., x- and y-edges). The improvement was performed by solving magnetostatic Maxwell's equations for an air- or iron-core coil supplied by a direct current. To evaluate the efficacy of the proposed technique, the magnetic flux density distributions have been compared with those obtained by the 2-D finite-element analysis (FEA). The semi-analytical results are in quite satisfying agreement with those obtained by the 2-D FEA, considering both amplitude and waveform.

Keywords: air- or iron-core coil; Cartesian coordinates; Fourier analysis; two-dimensional; saturation effect; subdomain technique

1. Introduction

1.1. Context of this Paper

Generally, the modeling of the electromagnetic field distribution is a key step in the design process for developing electromechanical systems. Although there are a lot of papers in this area, the modeling approach is still a challenging and attractive research topic. Some comprehensive reviews on the models of electrical machines for magnetic field calculations can be found in [1–6], and their references, with their (dis)advantages. The modeling techniques can thus be classified in various categories:

- Graphical method of **Lehmann** [7];
- Numerical methods (i.e., the finite-element, finite-difference or boundary-element analysis) [8–12];
- Electrical/Thermal/Magnetic equivalent circuit (EEC/TEC/MEC) [13–16];
- Schwarz-Christoffel (SC) mapping method [17–19];
- Maxwell-Fourier methods [10,18–22]: i) Multi-layers models, and ii) Subdomain technique.

The graphical method of **Lehmann**, which determines the magnetic field distribution in all parts of an electrical machine even when the machine is saturated, has been forgotten to the detriment of other methods, mainly numerical. In the past few decades, numerical modeling techniques have been applied to electromechanical systems analysis. These methods are precise and take into account the exact/simplified geometry, the nonlinear *B(H)* curve, the rotor motion,... The most accurate models are the three-dimensional numerical methods. Nevertheless, these approaches are time-consuming and not suitable for the optimization problems. In [23,24], it is possible to optimize

electromagnetic systems from numerical methods. Nowadays, in order to reduce the computation time, hybrid numerical methods can be developed [25–27]. The actual design works are mainly based on (semi-)analytical models (i.e., EEC/TEC/MEC, SC mapping and Maxwell-Fourier methods). Indeed, under certain assumptions, these models have the advantage to be explicit/accurate/fast. Moreover, they allow us to take into account rigorously the slotting effect in the electrical machines as well as various electromagnetic domains with(out) the current penetration effect in the conductive materials. Except in the numerical methods and nonlinear MEC, the saturation effect remains one of the scientific challenges in the modeling. **Tiegna *et al.* (2013)** [5] wrote: *"No examples of analytical models based on the formal solution of Maxwell's equations which take into account local magnetic saturation are available to date"*. Thus, in this paper, the main scientific focus will be on the consideration of iron in Maxwell-Fourier methods.

1.2. State-of-the-Art: Saturation in Maxwell-Fourier Methods

Very few works have included the iron or the saturation effect in Maxwell-Fourier methods due to variation of the material properties (e.g., in case of stator and/or rotor slotting, buried magnets,...). The most significant assumptions is defined by: *"The iron parts (i.e., the teeth and the back-iron) are considered to the infinitely permeable, i.e.,* $\mu_{iron} \rightarrow +\infty$*, so that the saturation effect is neglected"*. It results in an overestimation of the magnetic flux and, consequently, the electromagnetic performances (e.g., the back EMF, the electromagnetic torque, the efficiency). Thus, consideration of iron in the modeling is a mandatory task in order to have a reliable estimation of the electromechanical systems behavior.

Existing models in electrical machines, based on Maxwell's electromagnetic field equations, taking into account the iron parts with(out) the nonlinear *B(H)* curve are:

- *Multi-layers models*:
  - *Carter's coefficient*: The slotted machine is transformed into a slotless equivalent structure by applying the usual Carter's coefficient [28]. Generally, the armature slotting is taken into account through the SC mapping method. The analytical magnetic field distribution is determined in five or six homogeneous layers (i.e., exterior, slotless stator, winding/air-gap, magnets, and rotor) [29–31]. In [29], the magnetic permeabilities in stator/rotor iron cores have a constant value corresponding to linear zone of the *B(H)* curve. An iterative technique to include the nonlinear properties of core material has been developed in [30] (for a no-load operation) and [31] (for a load operation whose the source term in the slot caused by the armature currents is represented by a winding current region over the stator slot-isthmus). In this type of modeling, the local distribution of flux densities in the teeth and slots is neglected. However, by calculating the flux entering the stator surface from the air-gap magnetic field and thus assuming uniform distribution of flux, the flux density in middle of the stator teeth can be obtained.
  - *Saturation coefficient*: It represents the ratio between the total magnetomotive force (MMF) required for the entire magnetic circuit and the air-gap MMF [32]. The main magnetic saturation is included in the saturation factor, in an iterative way, by using the nonlinear *B(H)* curve. The saturation effect is accounted for by modifying the air-gap length [32–34] or by changing the physical properties of magnets (in this case, the saturated load operation is calculated by considering an equivalent no-load operation with a fictitious magnet having a remanent flux density that creates the same MMF as the one created by both real magnet and stator MMF) [35]. The analytical magnetic field distribution is mainly determined in one or two regions (viz., air-gap or air-gap/magnets) of slotless machines by applying the Carter's coefficient [32]. The slotting effect can be neglected [32,35] or taken into account through the SC mapping method [33,34]. The magnetic fluxes in the stator/rotor iron cores are obtained from the air-gap magnetic field [32,33,35] or/and with a simple MEC [34]. This technique

Preprints (www.preprints.org) | NOT PEER-REVIEWED | Posted: 27 September 2016 doi:10.20944/preprints201609.0106.v1

has been applied to surface-mounted/-inset magnets machines [32–35], surface-inset magnet machines [33], and others electrical machines.

- *Concept wave impedance*: They are based on a direct solution of Maxwell's field equations in homogeneous multi-layers of magnetic material properties, viz., the magnetic permeability and the electrical conductivity. This approach, developed by **Mishkin (1953)** [36], was first applied to squirrel-cage induction machine in Cartesian coordinates with three-layers (i.e., stator slotting, air-gap, and rotor slotting). It was used and enhanced by many authors, viz.,
  - simplification of the electromagnetic theory [37];
  - extended with an infinite number of layers [38];
  - converted into equivalent circuits and terminal impedance [39];
  - included the curvature effect with the magnetizing current [40];
  - incorporated spatial harmonics in the multi-layers theory by considering isotropic and anisotropic (e.g., laminated, composite, and toothed) regions [41,42];
  - introduced the nonlinear B(H) curve in homogenous layers by an iterative procedure [43, 44];
  - taking account of the effect of slot openings [45], i.e., the multi-layers model is combined with the subdomain technique for slotted structures by assuming infinitely permeable tooth tips;
  - included the current penetration effect in conductive layers [43,46]. The analytical solution for the electromagnetic field in conductive layers is then defined by Bessel functions.
- *Convolution theorem*: The electrical machine is divided into an infinite number of (in)homogeneous layers. The permeability in the stator and/or rotor slotting is represented by a complex Fourier series along the direction of permeability variation The permeability variation in the direction of the periodicity is directly included into the solution of the magnetic field equation. The resulting formulation, based on a direct solution of Maxwell's field equations using the Cauchy product theorem (i.e., the discrete convolution of two infinite series), is completely defined in terms of complex Fourier series [47]. Recently, [48] extended this modeling taking into account the nonlinear *B(H)* curve in each soft-magnetic section by an iterative procedure. For the moment, this technique has been applied to a switched reluctance machine [48] and a synchronous reluctance machine [49].

- *Hybrid models*: The analytical solution can be combined with numerical methods [50–53] or (non)linear MEC [54–63]. Usually, the analytical solution is established in uniform regions of very low permeability (e.g., air-gap, and magnets) and other methods are sought in regions where magnetic saturation cannot be neglected (i.e., the stator and/or rotor iron cores).

1.3. Objectives of this Paper

To the best author's knowledge, in the literature, there is no (semi-)analytical model based on the subdomain technique that taking into account of iron parts with(out) the nonlinear *B(H)* curve. Thus, the work in this paper takes part in the development and improvement of the subdomain technique on this scientific topic.

The disadvantage of multi-layers models, apart from using the concept wave impedance, is that it does not give a very accurate description of the local magnetic field distribution. In the harmonic modeling technique using the convolution theorem, convergence problems due to the truncated Fourier series around the soft-magnetic material discontinuities may exist [47–49]. Except in multi-layers models using the conception wave impedance, the electrical conductivity is assumed to be zero. The new approach developed in this paper allows the local distribution of flux densities in the iron parts, does not have numerical convergence problems, and would easily introduce the current penetration effect in the conductive materials. **Section 2** presents this new scientific contribution based on the subdomain technique. It was performed by solving 2-D magnetostatic Maxwell's

Preprints (www.preprints.org) | NOT PEER-REVIEWED | Posted: 27 September 2016 doi:10.20944/preprints201609.0106.v1

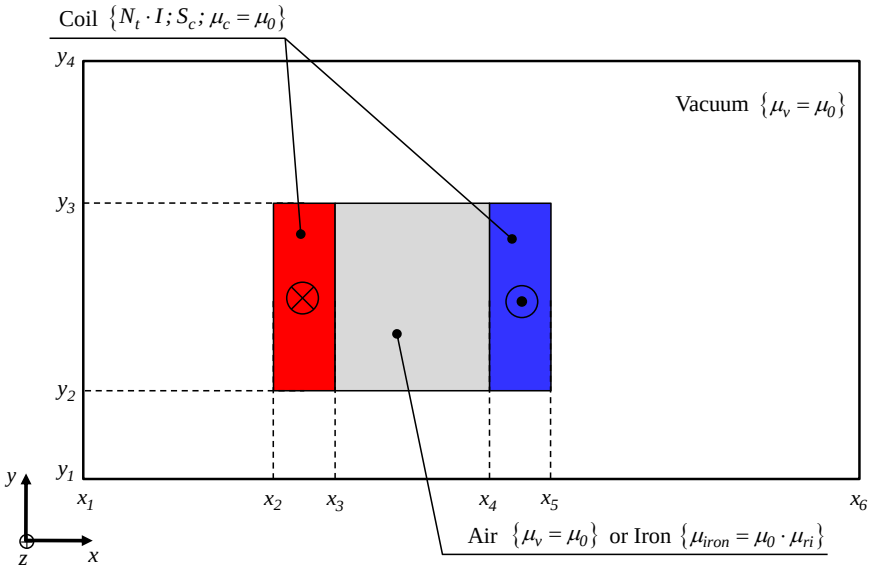

Figure 1. Air- or iron-core coil.

equations in Cartesian coordinates (x, y) for an air- or iron-core coil supplied by a direct current. The subdomains connection is carried out in the two directions (i.e., x- and y-edges). The iron magnetic permeability is constant corresponding to linear zone of the initial magnetization curve. Nevertheless, as in [48], it should be mentioned that the material properties could be updated iteratively to take the nonlinear *B(H)* curve of the material into account. However, this is beyond the scope of the paper. In **Section 3**, in order to evaluate the efficacy of the proposed technique, the magnetic flux density distributions have been compared with those obtained by the 2-D FEA [8]. The comparisons are very satisfying in amplitudes and waveforms.

This major scientific contribution could be applied to rotating and/or linear electrical machines with(out) magnets supplied by a direct current or alternate current (with any waveforms) whose the analysis would be based on a 2-D semi-analytical model in Cartesian coordinates (e.g., plane linear machines, axial-flux machines,...).

2. A 2-D Subdomain Technique of Magnetic Field

2.1. Problem Description and Assumptions

The application example, namely an air- or iron-core coil, with the geometrical and physical parameters is illustrated in Figure 1. The system consists of a coil with N_t turns of the copper wire which is supply by a direct current I. The direction of current in the conductor is defined by $\otimes$ for the forward conductor and $\odot$ for return conductor. The material in the middle of the coil can be air or iron. The system is surrounded by the vacuum via an infinite box.

The 2-D magnetic field distribution in the air- or iron-core coil has been studied in Cartesian coordinates (x, y) by solving magnetostatic Maxwell's equations from subdomain technique. In this analysis, the magnetic field solution is based on the following simplifying assumptions:

- The end-effects are neglected (i.e., that the magnetic variables are independent of z);
- The electrical conductivities of materials are assumed to be null (i.e., the eddy-currents induced in the copper/iron are neglected);
- The magnetic materials are considered as isotropic (i.e., the permeability can be assumed the same in the two directions);
- The saturation effect is taken into account with a constant magnetic permeability corresponding to linear zone of the *B(H)* curve (i.e., the initial magnetization curve).

Preprints (www.preprints.org) | NOT PEER-REVIEWED | Posted: 27 September 2016 doi:10.20944/preprints201609.0106.v1

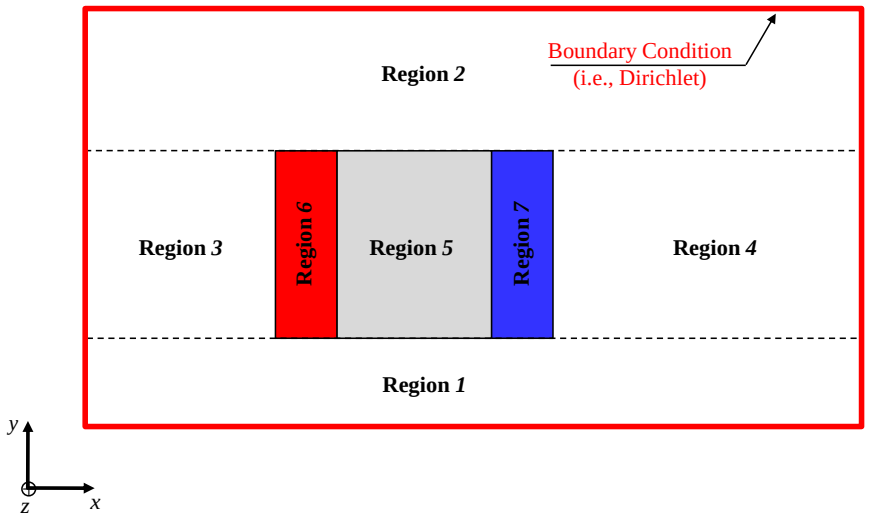

Figure 2. Subdomains in the air- or iron-core coil.

2.2. Problem Discretization in Subdomains

As shown in Figure 2, the problem domain is divided into 7 subdomains with $\mu = C^{st}$. The vacuum around to the air- or iron-core coil is defined by 4 regions, i.e.,

- Region 1 $\{\forall x \wedge y \in [y_1,\ y_2]\}$ with $\mu_1 = \mu_v$;
- Region 2 $\{\forall x \wedge y \in [y_3,\ y_4]\}$ with $\mu_2 = \mu_v$;
- Region 3 $\{x \in [x_1,\ x_2] \wedge y \in [y_2,\ y_3]\}$ with $\mu_3 = \mu_v$;
- Region 4 $\{x \in [x_5,\ x_6] \wedge y \in [y_2,\ y_3]\}$ with $\mu_4 = \mu_v$.

The air or iron in the middle of the coil is defined by the Region 5 $\{x \in [x_2,\ x_3] \wedge y \in [y_2,\ y_3]\}$ with $\mu_5 = \mu_v$ for the air or $\mu_5 = \mu_{iron}$ for the iron. The coil (i.e., forward and return conductors) is defined by 2 regions, i.e.,

- Region 6 $\{x \in [x_2,\ x_3] \wedge y \in [y_2,\ y_3]\}$ with $\mu_6 = \mu_c$;
- Region 7 $\{x \in [x_4,\ x_5] \wedge y \in [y_2,\ y_3]\}$ with $\mu_7 = \mu_c$.

2.3. Governing Partial Differential Equations in Cartesian Coordinates

According to (A.4) [see **Appendix A**], the 2-D magnetic vector potential distribution in Cartesian coordinates (x, y) is governed by the Laplace's equation in Regions j with $j = \{1,\ \ldots,\ 5\}$, i.e.,

$$\Delta A_{zj} = \frac{\partial^2 A_{zj}}{\partial x^2} + \frac{\partial^2 A_{zj}}{\partial y^2} = 0, \tag{1}$$

and the Poisson's equation in Regions k with $k = \{6,\ 7\}$, i.e.,

$$\Delta A_{zk} = \frac{\partial^2 A_{zk}}{\partial x^2} + \frac{\partial^2 A_{zk}}{\partial y^2} = -\mu_k \cdot J_{zk}, \tag{2a}$$

where J_{zk} represents the current density (due to supply currents) which is defined by

$$J_{zk} = C_k \cdot \frac{N_t \cdot I}{S_c}, \tag{2b}$$

in which S_c is the conductor surface, and C_k is the coefficient for the direction of current in the conductor (e.g., with $C_6 = 1$ for the forward conductor and $C_7 = -1$ for return conductor).

Preprints (www.preprints.org) | NOT PEER-REVIEWED | Posted: 27 September 2016 doi:10.20944/preprints201609.0106.v1

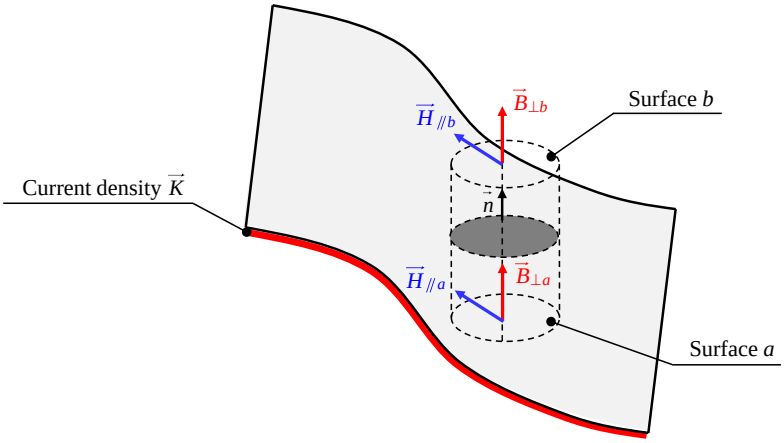

Figure 3. Boundary conditions at the interface of two surfaces.

According to the method of separation of variables, it is interesting to note that $A_{z\bullet}$ can be decomposed into two potentials according to the two directions [see **Appendix A**], i.e., $A^x_{z\bullet}$ for the x-edges (A.5b) and $A^y_{z\bullet}$ for the y-edges (A.5c). The periodicity of $A^x_{z\bullet}$ and $A^x_{z\bullet}$ are respectively defined by $\beta\bullet_{h\bullet}$ and $\lambda\bullet_{h\bullet}$ with $h\bullet$ and $n\bullet$ the spatial harmonic orders.

2.4. Boundary Conditions

2.4.1. Reminder on the Boundary Conditions at the Interface of Two Surfaces

In electromagnetic, as shown in Figure 3, the magnetic field $\vec{H}$ obeys Ampère's continuity condition,

$$\vec{n} \times \left(\vec{H}_{\|a} - \vec{H}_{\|b} \right) = \vec{K}, \tag{3a}$$

where $\vec{n}$ is the unit vector normal to the boundary between two surfaces, $\vec{H}_{\|}$ the parallel component of $\vec{H}$ on one side of the interface, and $\vec{K}$ the current density at the surface of the interface.

At this same surface, the magnetic flux continuity condition also applies

$$\vec{n} \cdot \left(\vec{B}_{\perp a} - \vec{B}_{\perp b} \right) = 0 \quad \text{or} \quad \vec{A}_a - \vec{A}_b = 0, \tag{3b}$$

where $\vec{B}_{\perp}$ is the perpendicular component of $\vec{B}$ on one side of the interface. The Dirichlet condition on one surface is defined by

$$\vec{A}_a = 0 \quad \text{or} \quad \vec{A}_b = 0. \tag{3c}$$

2.4.2. Application to the Air- or Iron-Core Coil

On the outer boundaries for $(x_1 \wedge x_6,\ \forall y)$ and $(\forall x,\ y_1 \wedge y_4)$ [see Figure 2], the component of the magnetic vector potential satisfies the Dirichlet boundary condition, i.e., (3c). By applying (3) and using (A.2) [see **Appendix A**], the respective boundaries at the interface between the various regions are illustrated in Figure 4.

2.5. General Solutions

2.5.1. Region 1

The general solution of A_{z1}, B_{x1} and B_{y1} are determined by the particular case of the *case-study no 1 "A_z imposed on all edges of a region"* in the **Appendix B**. The boundary conditions on the y-edges of

Preprints (www.preprints.org) | NOT PEER-REVIEWED | Posted: 27 September 2016 doi:10.20944/preprints201609.0106.v1

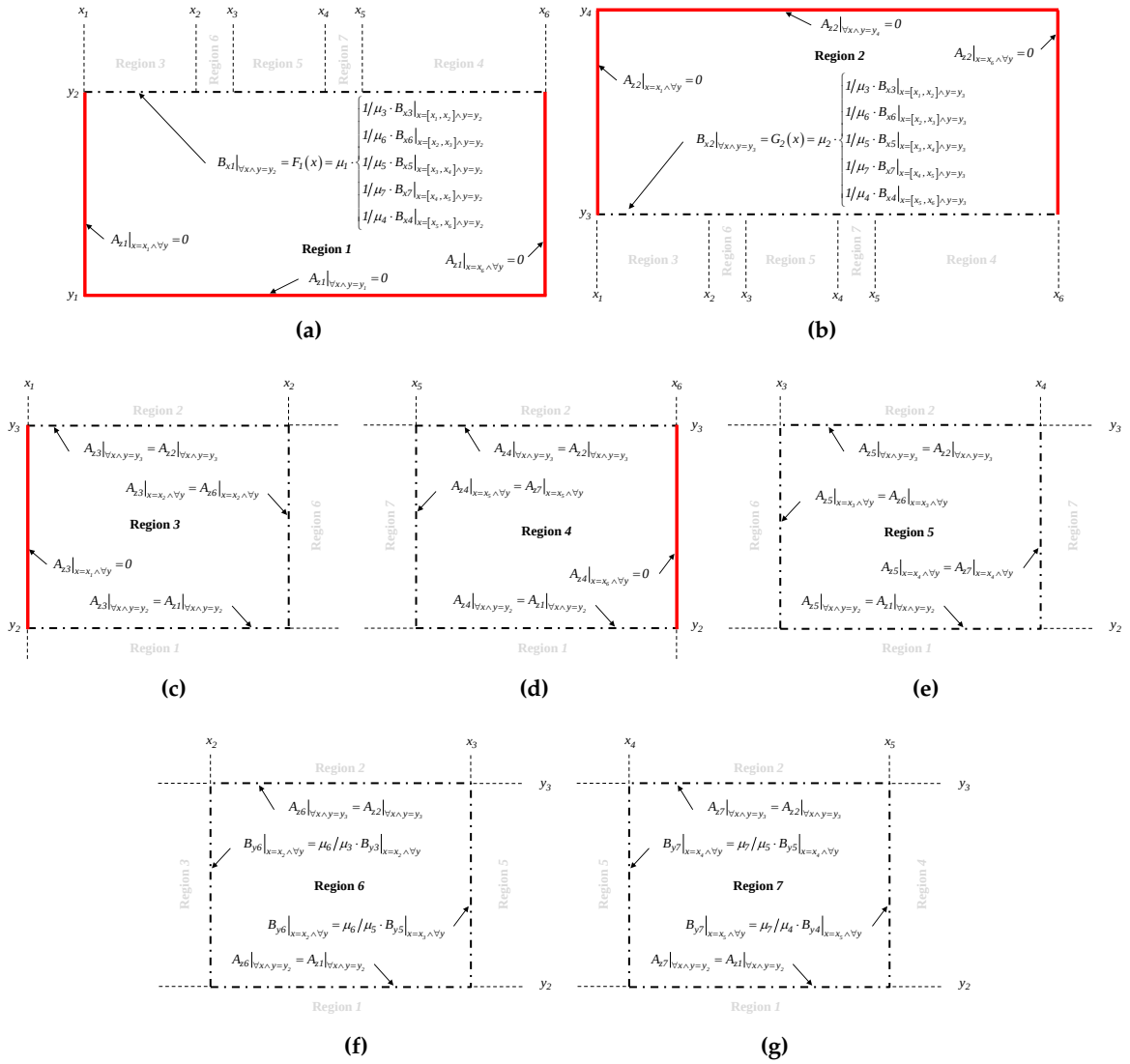

Figure 4. Boundary conditions in subdomains: **(a)** Region 1, **(b)** Region 2, **(c)** Region 3, **(d)** Region 4, **(e)** Region 5, **(f)** Region 6, and **(g)** Region 7.

the region [see Figure 4a] are met by posing $c_h^x = 0$ in (B.4). Therefore, the magnetic vector potential A_{z1}, which is a solution of (1) satisfying the boundary conditions of Figure 4a, is defined by

$$A_{z1} = \sum_{h1=1}^{\infty} \frac{d1_{h1}^x}{\beta 1_{h1}} \cdot \frac{\mathrm{sh}\left[\beta 1_{h1} \cdot (y - y_1)\right]}{ch\left(\beta 1_{h1} \cdot \tau_{y1}\right)} \cdot \sin\left[\beta 1_{h1} \cdot (x - x_1)\right], \tag{4}$$

the components of $\overrightarrow{B}_1 = \{B_{x1}; B_{y1}; 0\}$ by

$$B_{x1} = \sum_{h1=1}^{\infty} d1_{h1}^x \cdot \frac{ch\left[\beta 1_{h1} \cdot (y - y_1)\right]}{ch\left(\beta 1_{h1} \cdot \tau_{y1}\right)} \cdot \sin\left[\beta 1_{h1} \cdot (x - x_1)\right], \tag{5}$$

$$B_{y1} = -\sum_{h1=1}^{\infty} d1_{h1}^x \cdot \frac{\mathrm{sh}\left[\beta 1_{h1} \cdot (y - y_1)\right]}{ch\left(\beta 1_{h1} \cdot \tau_{y1}\right)} \cdot \cos\left[\beta 1_{h1} \cdot (x - x_1)\right], \tag{6}$$

where $h1$ is the spatial harmonic orders in Region 1, $d1_{h1}^x$ the integration constant, $\beta 1_{h1} = h1 \cdot \pi / \tau_{x1}$, and $\tau_{x1} = x_6 - x_1$ & $\tau_{y1} = y_2 - y_1$.

Preprints (www.preprints.org) | NOT PEER-REVIEWED | Posted: 27 September 2016 doi:10.20944/preprints201609.0106.v1

The coefficient $d1^x_{h1}$ is determined using a Fourier series expansion of $F_1(x)$ [see Figure 4a] over the interval $x = [x_1,\ x_6] = [x_1,\ x_1 + \tau_{x1}]$:

$$d1^x_{h1} = \frac{2}{\tau_{x1}} \cdot \int_{x_1}^{x_1+\tau_{x1}} F_1(x) \cdot \sin\left[\beta 1_{h1} \cdot (x - x_1)\right] \cdot dx. \tag{7}$$

The expression of $d1^x_{h1}$ is developed in the **Appendix C**.

2.5.2. Region 2

The same method than Region 1 is used to find the solution in Region 2. By posing $d^x_h = 0$ in (B.4) [see **Appendix B**], the magnetic vector potential A_{z2}, which is a solution of (1) satisfying the boundary conditions of Figure 4b, is defined by

$$A_{z2} = -\sum_{h2=1}^{\infty} \frac{c2^x_{h2}}{\beta 2_{h2}} \cdot \frac{sh\left[\beta 2_{h2} \cdot (y_4 - y)\right]}{ch\left(\beta 2_{h2} \cdot \tau_{y2}\right)} \cdot \sin\left[\beta 2_{h2} \cdot (x - x_1)\right], \tag{8}$$

the components of $\overrightarrow{B}_2 = \{B_{x2}; B_{y2}; 0\}$ by

$$B_{x2} = \sum_{h2=1}^{\infty} c2^x_{h2} \cdot \frac{ch\left[\beta 2_{h2} \cdot (y_4 - y)\right]}{ch\left(\beta 2_{h2} \cdot \tau_{y2}\right)} \cdot \sin\left[\beta 2_{h2} \cdot (x - x_1)\right], \tag{9}$$

$$B_{y2} = \sum_{h2=1}^{\infty} c2^x_{h2} \cdot \frac{sh\left[\beta 2_{h2} \cdot (y_4 - y)\right]}{ch\left(\beta 2_{h2} \cdot \tau_{y2}\right)} \cdot \cos\left[\beta 2_{h2} \cdot (x - x_1)\right], \tag{10}$$

where $h2$ is the spatial harmonic orders in Region 2, $c2^x_{h2}$ the integration constant, $\beta 2_{h2} = h2 \cdot \pi / \tau_{x2}$, and $\tau_{x2} = x_6 - x_1$ & $\tau_{y2} = y_4 - y_3$.

The coefficient $c2^x_{h2}$ is determined using a Fourier series expansion of $G_2(x)$ [see Figure 4b] over the interval $x = [x_1,\ x_6] = [x_1,\ x_1 + \tau_{x2}]$:

$$c2^x_{h2} = \frac{2}{\tau_{x2}} \cdot \int_{x_1}^{x_1+\tau_{x2}} G_2(x) \cdot \sin\left[\beta 2_{h2} \cdot (x - x_1)\right] \cdot dx. \tag{11}$$

The expression of $c2^x_{h2}$ is developed in the **Appendix C**.

2.5.3. Region 3

The general solution of A_{z3}, B_{x3} and B_{y3} are determined by the *case-study no 1 "A_z imposed on all edges of a region"* in the **Appendix B**. The boundary conditions on the x-edges of the region [see Figure 4c] are met by posing $e^y_n = 0$ in (B.1)-(B.3). Therefore, the magnetic vector potential A_{z3}, which is a solution of (1) satisfying the boundary conditions of Figure 4c, is defined by

$$A_{z3} = A^x_{z3} + A^y_{z3}, \tag{12a}$$

$$A^x_{z3} = \sum_{h3=1}^{\infty} \left\{ \frac{c3^x_{h3}}{\beta 3_{h3}} \cdot \frac{sh\left[\beta 3_{h3} \cdot (y_3 - y)\right]}{\mathrm{sh}\left(\beta 3_{h3} \cdot \tau_{y3}\right)} + \frac{d3^x_{h3}}{\beta 3_{h3}} \cdot \frac{\mathrm{sh}\left[\beta 3_{h3} \cdot (y - y_2)\right]}{\mathrm{sh}\left(\beta 3_{h3} \cdot \tau_{y3}\right)} \right\} \cdot \sin\left[\beta 3_{h3} \cdot (x - x_1)\right], \tag{12b}$$

$$A^y_{z3} = \sum_{n3=1}^{\infty} \frac{f3^y_{n3}}{\lambda 3_{n3}} \cdot \frac{sh\left[\lambda 3_{n3} \cdot (x - x_1)\right]}{sh\left(\lambda 3_{n3} \cdot \tau_{x3}\right)} \cdot \sin\left[\lambda 3_{n3} \cdot (y - y_2)\right], \tag{12c}$$

the x-component of $\overrightarrow{B}_3$ by

$$B_{x3} = B^x_{x3} + B^y_{x3}, \tag{13a}$$

Preprints (www.preprints.org) | NOT PEER-REVIEWED | Posted: 27 September 2016 doi:10.20944/preprints201609.0106.v1

$$B_{x3}^{x} = \sum_{h3=1}^{\infty} \left\{ -c3_{h3}^{x} \cdot \frac{ch\left[\beta 3_{h3} \cdot (y_3 - y)\right]}{\mathrm{sh}\left(\beta 3_{h3} \cdot \tau_{y3}\right)} + d3_{h3}^{x} \cdot \frac{ch\left[\beta 3_{h3} \cdot (y - y_2)\right]}{\mathrm{sh}\left(\beta 3_{h3} \cdot \tau_{y3}\right)} \right\} \cdot \sin\left[\beta 3_{h3} \cdot (x - x_1)\right], \quad (13b)$$

$$B_{x3}^{y} = \sum_{n3=1}^{\infty} f3_{n3}^{y} \cdot \frac{sh\left[\lambda 3_{n3} \cdot (x - x_1)\right]}{sh\left(\lambda 3_{n3} \cdot \tau_{x3}\right)} \cdot \cos\left[\lambda 3_{n3} \cdot (y - y_2)\right], \quad (13c)$$

the y-component of $\overrightarrow{B}_3$ by

$$B_{y3} = B_{y3}^{x} + B_{y3}^{y}, \quad (14a)$$

$$B_{y3}^{x} = -\sum_{h3=1}^{\infty} \left\{ c3_{h3}^{x} \cdot \frac{sh\left[\beta 3_{h3} \cdot (y_3 - y)\right]}{\mathrm{sh}\left(\beta 3_{h3} \cdot \tau_{y3}\right)} + d3_{h3}^{x} \cdot \frac{\mathrm{sh}\left[\beta 3_{h3} \cdot (y - y_2)\right]}{\mathrm{sh}\left(\beta 3_{h3} \cdot \tau_{y3}\right)} \right\} \cdot \cos\left[\beta 3_{h3} \cdot (x - x_1)\right], \quad (14b)$$

$$B_{y3}^{y} = -\sum_{n3=1}^{\infty} f3_{n3}^{y} \cdot \frac{ch\left[\lambda 3_{n3} \cdot (x - x_1)\right]}{sh\left(\lambda 3_{n3} \cdot \tau_{x3}\right)} \cdot \sin\left[\lambda 3_{n3} \cdot (y - y_2)\right], \quad (14c)$$

where $h3$ & $n3$ are the spatial harmonic orders in Region 3; $c3_{h3}^{x}$, $d3_{h3}^{x}$ and $f3_{n3}^{x}$ the integration constants; $\beta 3_{h3} = h3 \cdot \pi / \tau_{x3}$, and $\tau_{x3} = x_2 - x_1$; and $\lambda 3_{n3} = n3 \cdot \pi / \tau_{y3}$ with $\tau_{y3} = y_3 - y_2$.

The coefficients $c3_{h3}^{x}$ and $d3_{h3}^{x}$ are respectively determined using Fourier series expansion of $A_{z1}|_{\forall x \wedge y = y_2}$ and $A_{z2}|_{\forall x \wedge y = y_3}$ [see Figure 4c] over the interval $x = [x_1,\ x_2] = [x_1,\ x_1 + \tau_{x3}]$:

$$c3_{h3}^{x} = \frac{2}{\tau_{x3}} \cdot \int_{x_1}^{x_1 + \tau_{x3}} \beta 3_{h3} \cdot A_{z1}|_{y = y_2} \cdot \sin\left[\beta 3_{h3} \cdot (x - x_1)\right] \cdot dx, \quad (15a)$$

$$d3_{h3}^{x} = \frac{2}{\tau_{x3}} \cdot \int_{x_1}^{x_1 + \tau_{x3}} \beta 3_{h3} \cdot A_{z2}|_{y = y_3} \cdot \sin\left[\beta 3_{h3} \cdot (x - x_1)\right] \cdot dx. \quad (15b)$$

The coefficient $f3_{n3}^{y}$ is determined using a Fourier series expansion of $A_{z6}|_{x = x_2 \wedge \forall y}$ [see Figure 4c] over the interval $y = [y_2,\ y_3] = [y_2,\ y_2 + \tau_{y3}]$:

$$f3_{n3}^{y} = \frac{2}{\tau_{y3}} \cdot \int_{y_2}^{y_2 + \tau_{y3}} \lambda 3_{n3} \cdot A_{z6}|_{x = x_2} \cdot \sin\left[\lambda 3_{n3} \cdot (y - y_2)\right] \cdot dy. \quad (16)$$

The expression of $c3_{h3}^{x}$, $d3_{h3}^{x}$ and $f3_{n3}^{y}$ are developed in the **Appendix C**.

2.5.4. Region 4

The same method than Region 3 is used to find the solution in Region 4. By posing $f_n^{y} = 0$ in (B.1)-(B.3) [see **Appendix B**], the magnetic vector potential A_{z4}, which is a solution of (1) satisfying the boundary conditions of Figure 4d, is defined by

$$A_{z4} = A_{z4}^{x} + A_{z4}^{y}, \quad (17a)$$

$$A_{z4}^{x} = \sum_{h4=1}^{\infty} \left\{ \frac{c4_{h4}^{x}}{\beta 4_{h4}} \cdot \frac{sh\left[\beta 4_{h4} \cdot (y_3 - y)\right]}{\mathrm{sh}\left(\beta 4_{h4} \cdot \tau_{y4}\right)} + \frac{d4_{h4}^{x}}{\beta 4_{h4}} \cdot \frac{\mathrm{sh}\left[\beta 4_{h4} \cdot (y - y_2)\right]}{\mathrm{sh}\left(\beta 4_{h4} \cdot \tau_{y4}\right)} \right\} \cdot \sin\left[\beta 4_{h4} \cdot (x - x_5)\right], \quad (17b)$$

$$A_{z4}^{y} = \sum_{n4=1}^{\infty} \frac{e4_{n4}^{y}}{\lambda 4_{n4}} \cdot \frac{sh\left[\lambda 4_{n4} \cdot (x_6 - x)\right]}{sh\left(\lambda 4_{n4} \cdot \tau_{x4}\right)} \cdot \sin\left[\lambda 4_{n4} \cdot (y - y_2)\right], \quad (17c)$$

the x-component of $\overrightarrow{B}_4$ by

$$B_{x4} = B_{x4}^{x} + B_{x4}^{y}, \quad (18a)$$

Preprints (www.preprints.org) | NOT PEER-REVIEWED | Posted: 27 September 2016 doi:10.20944/preprints201609.0106.v1

$$B_{x4}^{x} = \sum_{h4=1}^{\infty} \left\{ -c4_{h4}^{x} \cdot \frac{ch\left[\beta 4_{h4} \cdot (y_3 - y)\right]}{\mathrm{sh}\left(\beta 4_{h4} \cdot \tau_{y4}\right)} + d4_{h4}^{x} \cdot \frac{ch\left[\beta 4_{h4} \cdot (y - y_2)\right]}{\mathrm{sh}\left(\beta 4_{h4} \cdot \tau_{y4}\right)} \right\} \cdot \sin\left[\beta 4_{h4} \cdot (x - x_5)\right], \quad (18b)$$

$$B_{x4}^{y} = \sum_{n4=1}^{\infty} e4_{n4}^{y} \cdot \frac{sh\left[\lambda 4_{n4} \cdot (x_6 - x)\right]}{sh\left(\lambda 4_{n4} \cdot \tau_{x4}\right)} \cdot \cos\left[\lambda 4_{n4} \cdot (y - y_2)\right], \quad (18c)$$

the y-component of $\overrightarrow{B}_4$ by

$$B_{y4} = B_{y4}^{x} + B_{y4}^{y}, \quad (19a)$$

$$B_{y4}^{x} = -\sum_{h4=1}^{\infty} \left\{ c4_{h4}^{x} \cdot \frac{sh\left[\beta 4_{h4} \cdot (y_3 - y)\right]}{\mathrm{sh}\left(\beta 4_{h4} \cdot \tau_{y4}\right)} + d4_{h4}^{x} \cdot \frac{\mathrm{sh}\left[\beta 4_{h4} \cdot (y - y_2)\right]}{\mathrm{sh}\left(\beta 4_{h4} \cdot \tau_{y4}\right)} \right\} \cdot \cos\left[\beta 4_{h4} \cdot (x - x_5)\right], \quad (19b)$$

$$B_{y4}^{y} = \sum_{n4=1}^{\infty} e4_{n4}^{y} \cdot \frac{ch\left[\lambda 4_{n4} \cdot (x_6 - x)\right]}{sh\left(\lambda 4_{n4} \cdot \tau_{x4}\right)} \cdot \sin\left[\lambda 4_{n4} \cdot (y - y_2)\right], \quad (19c)$$

where $h4$ & $n4$ are the spatial harmonic orders in Region 4; $c4_{h4}^{x}$, $d4_{h4}^{x}$ and $e4_{n4}^{y}$ the integration constants; $\beta 4_{h4} = h4 \cdot \pi / \tau_{x4}$, and $\tau_{x4} = x_6 - x_5$; and $\lambda 4_{n4} = n4 \cdot \pi / \tau_{y4}$ with $\tau_{y4} = y_3 - y_2$.

The coefficients $c4_{h4}^{x}$ and $d4_{h4}^{x}$ are respectively determined using Fourier series expansion of $A_{z1}|_{\forall x \wedge y = y_2}$ and $A_{z2}|_{\forall x \wedge y = y_3}$ [see Figure 4d] over the interval $x = [x_5,\ x_6] = [x_5,\ x_5 + \tau_{x4}]$:

$$c4_{h4}^{x} = \frac{2}{\tau_{x4}} \cdot \int_{x_5}^{x_5 + \tau_{x4}} \beta 4_{h4} \cdot A_{z1}|_{y = y_2} \cdot \sin\left[\beta 4_{h4} \cdot (x - x_5)\right] \cdot dx, \quad (20a)$$

$$d4_{h4}^{x} = \frac{2}{\tau_{x4}} \cdot \int_{x_5}^{x_5 + \tau_{x4}} \beta 4_{h4} \cdot A_{z2}|_{y = y_3} \cdot \sin\left[\beta 4_{h4} \cdot (x - x_5)\right] \cdot dx. \quad (20b)$$

The coefficient $e4_{n4}^{y}$ is determined using a Fourier series expansion of $A_{z7}|_{x = x_5 \wedge \forall y}$ [see Figure 4d] over the interval $y = [y_2,\ y_3] = [y_2,\ y_2 + \tau_{y4}]$:

$$e4_{n4}^{y} = \frac{2}{\tau_{y4}} \cdot \int_{y_2}^{y_2 + \tau_{y4}} \lambda 4_{n4} \cdot A_{z7}|_{x = x_5} \cdot \sin\left[\lambda 4_{n4} \cdot (y - y_2)\right] \cdot dy. \quad (21)$$

The expression of $c4_{h4}^{x}$, $d4_{h4}^{x}$ and $e4_{n4}^{y}$ are developed in the **Appendix C**.

2.5.5. Region 5

According to *case-study no 1 "A_z imposed on all edges of a region"* in the **Appendix B**, the magnetic vector potential A_{z5}, which is a solution of (1) satisfying the boundary conditions of Figure 4e, is defined by

$$A_{z5} = A_{z5}^{x} + A_{z5}^{y}, \quad (22a)$$

$$A_{z5}^{x} = \sum_{h5=1}^{\infty} \left\{ \frac{c5_{h5}^{x}}{\beta 5_{h5}} \cdot \frac{sh\left[\beta 5_{h5} \cdot (y_3 - y)\right]}{\mathrm{sh}\left(\beta 5_{h5} \cdot \tau_{y5}\right)} + \frac{d5_{h5}^{x}}{\beta 5_{h5}} \cdot \frac{\mathrm{sh}\left[\beta 5_{h5} \cdot (y - y_2)\right]}{\mathrm{sh}\left(\beta 5_{h5} \cdot \tau_{y5}\right)} \right\} \cdot \sin\left[\beta 5_{h5} \cdot (x - x_3)\right], \quad (22b)$$

$$A_{z5}^{y} = \sum_{n5=1}^{\infty} \left\{ \frac{e5_{n5}^{y}}{\lambda 5_{n5}} \cdot \frac{sh\left[\lambda 5_{n5} \cdot (x_4 - x)\right]}{sh\left(\lambda 5_{n5} \cdot \tau_{x5}\right)} + \frac{f5_{n5}^{y}}{\lambda 5_{n5}} \cdot \frac{sh\left[\lambda 5_{n5} \cdot (x - x_3)\right]}{sh\left(\lambda 5_{n5} \cdot \tau_{x5}\right)} \right\} \cdot \sin\left[\lambda 5_{n5} \cdot (y - y_2)\right], \quad (22c)$$

the x-component of $\overrightarrow{B}_5$ by

$$B_{x5} = B_{x5}^{x} + B_{x5}^{y}, \quad (23a)$$

$$B_{x5}^{x} = \sum_{h5=1}^{\infty} \left\{ -c5_{h5}^{x} \cdot \frac{ch\left[\beta 5_{h5} \cdot (y_3 - y)\right]}{\mathrm{sh}\left(\beta 5_{h5} \cdot \tau_{y5}\right)} + d5_{h5}^{x} \cdot \frac{ch\left[\beta 5_{h5} \cdot (y - y_2)\right]}{\mathrm{sh}\left(\beta 5_{h5} \cdot \tau_{y5}\right)} \right\} \cdot \sin\left[\beta 5_{h5} \cdot (x - x_3)\right], \quad (23b)$$

Preprints (www.preprints.org) | NOT PEER-REVIEWED | Posted: 27 September 2016 doi:10.20944/preprints201609.0106.v1

$$B_{x5}^{y} = \sum_{n5=1}^{\infty} \left\{ e5_{n5}^{y} \cdot \frac{sh\left[\lambda 5_{n5} \cdot (x_4 - x)\right]}{sh\left(\lambda 5_{n5} \cdot \tau_{x5}\right)} + f5_{n5}^{y} \cdot \frac{sh\left[\lambda 5_{n5} \cdot (x - x_3)\right]}{sh\left(\lambda 5_{n5} \cdot \tau_{x5}\right)} \right\} \cdot \cos\left[\lambda 5_{n5} \cdot (y - y_2)\right], \tag{23c}$$

the y-component of $\overrightarrow{B}_5$ by

$$B_{y5} = B_{y5}^{x} + B_{y5}^{y}, \tag{24a}$$

$$B_{y5}^{x} = -\sum_{h5=1}^{\infty} \left\{ c5_{h5}^{x} \cdot \frac{sh\left[\beta 5_{h5} \cdot (y_3 - y)\right]}{\mathrm{sh}\left(\beta 5_{h5} \cdot \tau_{y5}\right)} + d5_{h5}^{x} \cdot \frac{\mathrm{sh}\left[\beta 5_{h5} \cdot (y - y_2)\right]}{\mathrm{sh}\left(\beta 5_{h5} \cdot \tau_{y5}\right)} \right\} \cdot \cos\left[\beta 5_{h5} \cdot (x - x_3)\right], \tag{24b}$$

$$B_{y5}^{y} = -\sum_{n5=1}^{\infty} \left\{ -e5_{n5}^{y} \cdot \frac{ch\left[\lambda_{n5} \cdot (x_4 - x)\right]}{sh\left(\lambda_{n5} \cdot \tau_{x5}\right)} + f5_{n5}^{y} \cdot \frac{ch\left[\lambda_{n5} \cdot (x - x_3)\right]}{sh\left(\lambda_{n5} \cdot \tau_{x5}\right)} \right\} \cdot \sin\left[\lambda_{n5} \cdot (y - y_2)\right], \tag{24c}$$

where $h5$ & $n5$ are the spatial harmonic orders in Region 5; $c5_{h5}^{x}$, $d5_{h5}^{x}$, $e5_{n5}^{y}$ and $f5_{n5}^{y}$ the integration constants; $\beta 5_{h5} = h5 \cdot \pi / \tau_{x5}$, and $\tau_{x5} = x_4 - x_3$; and $\lambda 5_{n5} = n5 \cdot \pi / \tau_{y5}$ with $\tau_{y5} = y_3 - y_2$.

The coefficients $c5_{h5}^{x}$ and $d5_{h5}^{x}$ are respectively determined using Fourier series expansion of $A_{z1}|_{\forall x \wedge y = y_2}$ and $A_{z2}|_{\forall x \wedge y = y_3}$ [see Figure 4e] over the interval $x = [x_3,\ x_5] = [x_3,\ x_3 + \tau_{x5}]$:

$$c5_{h5}^{x} = \frac{2}{\tau_{x5}} \cdot \int_{x_3}^{x_3 + \tau_{x5}} \beta 5_{h5} \cdot A_{z1}|_{y = y_2} \cdot \sin\left[\beta 5_{h5} \cdot (x - x_3)\right] \cdot dx, \tag{25a}$$

$$d5_{h5}^{x} = \frac{2}{\tau_{x5}} \cdot \int_{x_3}^{x_3 + \tau_{x5}} \beta 5_{h5} \cdot A_{z2}|_{y = y_3} \cdot \sin\left[\beta 5_{h5} \cdot (x - x_3)\right] \cdot dx. \tag{25b}$$

The coefficient $e5_{n5}^{y}$ and $f5_{n5}^{y}$ are respectively determined using a Fourier series expansion of $A_{z6}|_{x = x_3 \wedge \forall y}$ and $A_{z7}|_{x = x_4 \wedge \forall y}$ [see Figure 4e] over the interval $y = [y_2,\ y_3] = [y_2,\ y_2 + \tau_{y5}]$:

$$e5_{n5}^{y} = \frac{2}{\tau_{y5}} \cdot \int_{y_2}^{y_2 + \tau_{y5}} \lambda 5_{n5} \cdot A_{z6}|_{x = x_3} \cdot \sin\left[\lambda 5_{n5} \cdot (y - y_2)\right] \cdot dy, \tag{26a}$$

$$f5_{n5}^{y} = \frac{2}{\tau_{y5}} \cdot \int_{y_2}^{y_2 + \tau_{y5}} \lambda 5_{n5} \cdot A_{z7}|_{x = x_4} \cdot \sin\left[\lambda 5_{n5} \cdot (y - y_2)\right] \cdot dy. \tag{26b}$$

The expression of $c5_{h5}^{x}$, $d5_{h5}^{x}$, $e5_{n5}^{y}$ and $f5_{n5}^{y}$ are developed in the **Appendix C**.

2.5.6. Region 6

According to *case-study no 2 "B_y and A_z are respectively imposed on x- and y-edges of a region"* in the **Appendix B**, the magnetic vector potential A_{z6}, which is a solution of (2) satisfying the boundary conditions of Figure 4f, is defined by

$$A_{z6} = A_{z6}^{x} + A_{z6}^{y} + A_{zP6}, \tag{27a}$$

$$A_{z6}^{x} = \left| \begin{array}{l} (y_3 - y) \cdot c6_0^{x} + (y - y_2) \cdot d6_0^{x} \\ \cdots + \sum_{h6=1}^{\infty} \left\{ \frac{c6_{h6}^{x}}{\beta 6_{h6}} \cdot \frac{sh\left[\beta 6_{h6} \cdot (y_3 - y)\right]}{\mathrm{sh}\left(\beta 6_{h6} \cdot \tau_{y6}\right)} + \frac{d6_{h6}^{x}}{\beta 6_{h6}} \cdot \frac{\mathrm{sh}\left[\beta 6_{h6} \cdot (y - y_2)\right]}{\mathrm{sh}\left(\beta 6_{h6} \cdot \tau_{y6}\right)} \right\} \cdot \cos\left[\beta 6_{h6} \cdot (x - x_2)\right] \end{array} \right., \tag{27b}$$

$$A_{z6}^{y} = -\sum_{n6=1}^{\infty} \left\{ \frac{e6_{n6}^{y}}{\lambda 6_{n6}} \cdot \frac{\mathrm{ch}\left[\lambda 6_{n6} \cdot (x - x_2)\right]}{sh\left(\lambda 6_{n6} \cdot \tau_{x6}\right)} - \frac{f6_{n6}^{y}}{\lambda 6_{n6}} \cdot \frac{ch\left[\lambda 6_{n6} \cdot (x_3 - x)\right]}{sh\left(\lambda 6_{n6} \cdot \tau_{x6}\right)} \right\} \cdot \sin\left[\lambda 6_{n6} \cdot (y - y_2)\right]. \tag{27c}$$

Preprints (www.preprints.org) | NOT PEER-REVIEWED | Posted: 27 September 2016 doi:10.20944/preprints201609.0106.v1

Considering the form of the current density distribution, i.e., (2b), a particular solution A_{zP6} can be found as follows:

$$A_{zP6} = -\frac{1}{2} \cdot \mu_6 \cdot J_{z6} \cdot y^2. \tag{27d}$$

The x-component of $\overrightarrow{B}_6$ is defined by

$$B_{x6} = B_{x6}^x + B_{x6}^y + B_{xP6}, \tag{28a}$$

$$B_{x6}^x = \left| \begin{array}{l} -c6_0^x + d6_0^x \\ \cdots + \sum\limits_{h6=1}^{\infty} \left\{ -c6_{h6}^x \cdot \frac{ch[\beta 6_{h6} \cdot (y_3 - y)]}{\mathrm{sh}(\beta 6_{h6} \cdot \tau_{y6})} + d6_{h6}^x \cdot \frac{ch[\beta 6_{h6} \cdot (y - y_2)]}{\mathrm{sh}(\beta 6_{h6} \cdot \tau_{y6})} \right\} \cdot \cos\left[\beta 6_{h6} \cdot (x - x_2)\right] \end{array} \right., \tag{28b}$$

$$B_{x6}^y = -\sum_{n6=1}^{\infty} \left\{ e6_{n6}^y \cdot \frac{\mathrm{ch}\left[\lambda 6_{n6} \cdot (x - x_2)\right]}{sh\left(\lambda 6_{n6} \cdot \tau_{x6}\right)} - f6_{n6}^y \cdot \frac{ch\left[\lambda 6_{n6} \cdot (x_3 - x)\right]}{sh\left(\lambda 6_{n6} \cdot \tau_{x6}\right)} \right\} \cdot \cos\left[\lambda 6_{n6} \cdot (y - y_2)\right], \tag{28c}$$

$$B_{xP6} = \frac{\partial A_{zP6}}{\partial y} = -\mu_6 \cdot J_{z6} \cdot y, \tag{28d}$$

and the y-component of $\overrightarrow{B}_6$ by

$$B_{y6} = B_{y6}^x + B_{y6}^y + B_{yP6}, \tag{29a}$$

$$B_{y6}^x = \sum_{h6=1}^{\infty} \left\{ c6_{h6}^x \cdot \frac{sh\left[\beta 6_{h6} \cdot (y_3 - y)\right]}{\mathrm{sh}\left(\beta 6_{h6} \cdot \tau_{y6}\right)} + d6_{h6}^x \cdot \frac{\mathrm{sh}\left[\beta 6_{h6} \cdot (y - y_2)\right]}{\mathrm{sh}\left(\beta 6_{h6} \cdot \tau_{y6}\right)} \right\} \cdot \sin\left[\beta 6_{h6} \cdot (x - x_2)\right], \tag{29b}$$

$$B_{y6}^y = \sum_{n6=1}^{\infty} \left\{ e6_{n6}^y \cdot \frac{sh\left[\lambda 6_{n6} \cdot (x - x_2)\right]}{sh\left(\lambda 6_{n6} \cdot \tau_{x6}\right)} + f6_{n6}^y \cdot \frac{sh\left[\lambda 6_{n6} \cdot (x_3 - x)\right]}{sh\left(\lambda 6_{n6} \cdot \tau_{x6}\right)} \right\} \cdot \sin\left[\lambda 6_{n6} \cdot (y - y_2)\right], \tag{29c}$$

$$B_{yP6} = -\frac{\partial A_{zP6}}{\partial x} = 0, \tag{29d}$$

where $h6$ & $n6$ are the spatial harmonic orders in Region 6; $c6_0^x$, $d6_0^x$, $c6_{h6}^x$, $d6_{h6}^x$, $e6_{n6}^y$ and $f6_{n6}^y$ the integration constants; $\beta 6_{h6} = h6 \cdot \pi / \tau_{x6}$, and $\tau_{x6} = x_3 - x_2$; and $\lambda 6_{n6} = n6 \cdot \pi / \tau_{y6}$ with $\tau_{y6} = y_3 - y_2$.

The coefficients $c6_0^x$ & $c6_{h6}^x$ and $d6_0^x$ & $d6_{h6}^x$ are respectively determined using Fourier series expansion of $A_{z1}|_{\forall x \wedge y = y_2}$ and $A_{z2}|_{\forall x \wedge y = y_3}$ [see Figure 4f] over the interval $x = [x_2,\ x_3] = [x_2,\ x_2 + \tau_{x6}]$:

$$c6_0^x + \frac{1}{\tau_{y6}} \cdot A_{zP6}|_{y=y_2} = \frac{1}{\tau_{x6}} \cdot \int_{x_2}^{x_2+\tau_{x6}} \frac{1}{\tau_{y6}} \cdot A_{z1}|_{y=y_2} \cdot dx, \tag{30a}$$

$$c6_{h6}^x = \frac{2}{\tau_{x6}} \cdot \int_{x_2}^{x_2+\tau_{x6}} \beta 6_{h6} \cdot A_{z1}|_{y=y_2} \cdot \cos\left[\beta 6_{h6} \cdot (x - x_2)\right] \cdot dx, \tag{30b}$$

$$d6_0^x + \frac{1}{\tau_{y6}} \cdot A_{zP6}|_{y=y_3} = \frac{1}{\tau_{x6}} \cdot \int_{x_2}^{x_2+\tau_{x6}} \frac{1}{\tau_{y6}} \cdot A_{z2}|_{y=y_3} \cdot dx, \tag{30c}$$

$$d6_{h6}^x = \frac{2}{\tau_{x6}} \cdot \int_{x_2}^{x_2+\tau_{x6}} \beta 6_{h6} \cdot A_{z2}|_{y=y_3} \cdot \cos\left[\beta 6_{h6} \cdot (x - x_2)\right] \cdot dx. \tag{30d}$$

The coefficient $e6_{n6}^y$ and $f6_{n6}^y$ are respectively determined using a Fourier series expansion of $\mu_6/\mu_5 \cdot B_{y5}|_{x=x_3 \wedge \forall y}$ and $\mu_6/\mu_3 \cdot B_{y3}|_{x=x_2 \wedge \forall y}$ [see Figure 4f] over the interval $y = [y_2,\ y_3] = [y_2,\ y_2 + \tau_{y6}]$:

$$e6_{n6}^y = \frac{2}{\tau_{y6}} \cdot \int_{y_2}^{y_2+\tau_{y6}} \frac{\mu_6}{\mu_5} \cdot B_{y5}|_{x=x_3} \cdot \sin\left[\lambda 6_{n6} \cdot (y - y_2)\right] \cdot dy, \tag{31a}$$

Preprints (www.preprints.org) | NOT PEER-REVIEWED | Posted: 27 September 2016 doi:10.20944/preprints201609.0106.v1

$$f6^{y}_{n6} = \frac{2}{\tau_{y6}} \cdot \int_{y_2}^{y_2+\tau_{y6}} \frac{\mu_6}{\mu_3} \cdot B_{y3}\big|_{x=x_2} \cdot \sin\left[\lambda 6_{n6} \cdot (y - y_2)\right] \cdot dy. \tag{31b}$$

The expression of $c6^{x}_{0}$, $d6^{x}_{0}$, $c6^{x}_{h6}$, $d6^{x}_{h6}$, $e6^{y}_{n6}$ and $f6^{y}_{n6}$ are developed in the **Appendix C**.

2.5.7. Region 7

According to *case-study no 2 "B_y and A_z are respectively imposed on x- and y-edges of a region"* in the **Appendix B**, the magnetic vector potential A_{z7}, which is a solution of (2) satisfying the boundary conditions of Figure 4g, is defined by

$$A_{z7} = A^{x}_{z7} + A^{y}_{z7} + A_{zP7}, \tag{32a}$$

$$A^{x}_{z7} = \left| \begin{array}{l} (y_3 - y) \cdot c7^{x}_{0} + (y - y_2) \cdot d7^{x}_{0} \\ \cdots + \sum_{h7=1}^{\infty} \left\{ \frac{c7^{x}_{h7}}{\beta 7_{h7}} \cdot \frac{sh[\beta 7_{h7} \cdot (y_3 - y)]}{\mathrm{sh}\left(\beta 7_{h7} \cdot \tau_{y7}\right)} + \frac{d7^{x}_{h7}}{\beta 7_{h7}} \cdot \frac{\mathrm{sh}[\beta 7_{h7} \cdot (y - y_2)]}{\mathrm{sh}\left(\beta 7_{h7} \cdot \tau_{y7}\right)} \right\} \cdot \cos\left[\beta 7_{h7} \cdot (x - x_4)\right] \end{array} \right. , \tag{32b}$$

$$A^{y}_{z7} = -\sum_{n7=1}^{\infty} \left\{ \frac{e7^{y}_{n7}}{\lambda 7_{n7}} \cdot \frac{\mathrm{ch}\left[\lambda 7_{n7} \cdot (x - x_4)\right]}{sh\left(\lambda 7_{n7} \cdot \tau_{x7}\right)} - \frac{f7^{y}_{n7}}{\lambda 7_{n7}} \cdot \frac{ch\left[\lambda 7_{n7} \cdot (x_5 - x)\right]}{sh\left(\lambda 7_{n7} \cdot \tau_{x7}\right)} \right\} \cdot \sin\left[\lambda 7_{n7} \cdot (y - y_2)\right]. \tag{32c}$$

Considering the form of the current density distribution, i.e., (2b), a particular solution A_{zP7} can be found as follows:

$$A_{zP7} = -\frac{1}{2} \cdot \mu_7 \cdot J_{z7} \cdot y^2. \tag{32d}$$

The x-component of $\overrightarrow{B}_7$ is defined by

$$B_{x7} = B^{x}_{x7} + B^{y}_{x7} + B_{xP7}, \tag{33a}$$

$$B^{x}_{x7} = \left| \begin{array}{l} -c7^{x}_{0} + d7^{x}_{0} \\ \cdots + \sum_{h7=1}^{\infty} \left\{ -c7^{x}_{h7} \cdot \frac{ch[\beta 7_{h7} \cdot (y_3 - y)]}{\mathrm{sh}\left(\beta 7_{h7} \cdot \tau_{y7}\right)} + d7^{x}_{h7} \cdot \frac{ch[\beta 7_{h7} \cdot (y - y_2)]}{\mathrm{sh}\left(\beta 7_{h7} \cdot \tau_{y7}\right)} \right\} \cdot \cos\left[\beta 7_{h7} \cdot (x - x_4)\right] \end{array} \right. , \tag{33b}$$

$$B^{y}_{x7} = -\sum_{n7=1}^{\infty} \left\{ e7^{y}_{n7} \cdot \frac{\mathrm{ch}\left[\lambda 7_{n7} \cdot (x - x_4)\right]}{sh\left(\lambda 7_{n7} \cdot \tau_{x7}\right)} - f6^{y}_{n7} \cdot \frac{ch\left[\lambda 7_{n7} \cdot (x_5 - x)\right]}{sh\left(\lambda 7_{n7} \cdot \tau_{x7}\right)} \right\} \cdot \cos\left[\lambda 7_{n7} \cdot (y - y_2)\right], \tag{33c}$$

$$B_{xP7} = \frac{\partial A_{zP7}}{\partial y} = -\mu_7 \cdot J_{z7} \cdot y, \tag{33d}$$

and the y-component of $\overrightarrow{B}_7$ by

$$B_{y7} = B^{x}_{y7} + B^{y}_{y7} + B_{yP7}, \tag{34a}$$

$$B^{x}_{y7} = \sum_{h7=1}^{\infty} \left\{ c7^{x}_{h7} \cdot \frac{sh\left[\beta 7_{h7} \cdot (y_3 - y)\right]}{\mathrm{sh}\left(\beta 7_{h7} \cdot \tau_{y7}\right)} + d7^{x}_{h7} \cdot \frac{\mathrm{sh}\left[\beta 7_{h7} \cdot (y - y_2)\right]}{\mathrm{sh}\left(\beta 7_{h7} \cdot \tau_{y7}\right)} \right\} \cdot \sin\left[\beta 7_{h7} \cdot (x - x_4)\right], \tag{34b}$$

$$B^{y}_{y7} = \sum_{n7=1}^{\infty} \left\{ e7^{y}_{n7} \cdot \frac{sh\left[\lambda 7_{n7} \cdot (x - x_4)\right]}{sh\left(\lambda 7_{n7} \cdot \tau_{x7}\right)} + f7^{y}_{n7} \cdot \frac{sh\left[\lambda 7_{n7} \cdot (x_5 - x)\right]}{sh\left(\lambda 7_{n7} \cdot \tau_{x7}\right)} \right\} \cdot \sin\left[\lambda 7_{n7} \cdot (y - y_2)\right], \tag{34c}$$

$$B_{yP7} = -\frac{\partial A_{zP7}}{\partial x} = 0, \tag{34d}$$

where $h7$ & $n7$ are the spatial harmonic orders in Region 7; $c7^{x}_{0}$, $d7^{x}_{0}$, $c7^{x}_{h7}$, $d7^{x}_{h7}$, $e7^{y}_{n7}$ and $f7^{y}_{n7}$ the integration constants; $\beta 7_{h7} = h7 \cdot \pi / \tau_{x7}$, and $\tau_{x7} = x_5 - x_4$; and $\lambda 7_{n7} = n7 \cdot \pi / \tau_{y7}$ with $\tau_{y7} = y_3 - y_2$.

Preprints (www.preprints.org) | NOT PEER-REVIEWED | Posted: 27 September 2016 doi:10.20944/preprints201609.0106.v1

The coefficients $c7_0^x$ & $c7_{h7}^x$ and $d7_0^x$ & $d7_{h7}^x$ are respectively determined using Fourier series expansion of $A_{z1}|_{\forall x \wedge y=y_2}$ and $A_{z2}|_{\forall x \wedge y=y_3}$ [see Figure 4g] over the interval $x = [x_4,\ x_5] = [x_4,\ x_4 + \tau_{x7}]$:

$$c7_0^x + \frac{1}{\tau_{y7}} \cdot A_{zP7}|_{y=y_2} = \frac{1}{\tau_{x7}} \cdot \int_{x_4}^{x_4+\tau_{x7}} \frac{1}{\tau_{y7}} \cdot A_{z1}|_{y=y_2} \cdot dx, \tag{35a}$$

$$c7_{h7}^x = \frac{2}{\tau_{x7}} \cdot \int_{x_4}^{x_4+\tau_{x7}} \beta 7_{h7} \cdot A_{z1}|_{y=y_2} \cdot \cos\left[\beta 7_{h7} \cdot (x - x_4)\right] \cdot dx, \tag{35b}$$

$$d7_0^x + \frac{1}{\tau_{y7}} \cdot A_{zP7}|_{y=y_3} = \frac{1}{\tau_{x7}} \cdot \int_{x_4}^{x_4+\tau_{x7}} \frac{1}{\tau_{y7}} \cdot A_{z2}|_{y=y_3} \cdot dx, \tag{35c}$$

$$d7_{h7}^x = \frac{2}{\tau_{x7}} \cdot \int_{x_4}^{x_4+\tau_{x7}} \beta 7_{h7} \cdot A_{z2}|_{y=y_3} \cdot \cos\left[\beta 7_{h7} \cdot (x - x_4)\right] \cdot dx. \tag{35d}$$

The coefficient $e7_{n7}^y$ and $f7_{n7}^y$ are respectively determined using a Fourier series expansion of $\mu_7/\mu_4 \cdot B_{y4}|_{x=x_5 \wedge \forall y}$ and $\mu_7/\mu_5 \cdot B_{y5}|_{x=x_4 \wedge \forall y}$ [see Figure 4g] over the interval $y = [y_2,\ y_3] = [y_2,\ y_2 + \tau_{y7}]$:

$$e7_{n7}^y = \frac{2}{\tau_{y7}} \cdot \int_{y_2}^{y_2+\tau_{y7}} \frac{\mu_7}{\mu_4} \cdot B_{y4}|_{x=x_5} \cdot \sin\left[\lambda 7_{n7} \cdot (y - y_2)\right] \cdot dy, \tag{36a}$$

$$f7_{n7}^y = \frac{2}{\tau_{y7}} \cdot \int_{y_2}^{y_2+\tau_{y7}} \frac{\mu_7}{\mu_5} \cdot B_{y5}|_{x=x_4} \cdot \sin\left[\lambda 7_{n7} \cdot (y - y_2)\right] \cdot dy. \tag{36b}$$

The expression of $c7_0^x$, $d7_0^x$, $c7_{h7}^x$, $d7_{h7}^x$, $e7_{n7}^y$ and $f7_{n7}^y$ are developed in the **Appendix C**.

2.6. Solving of Cramer's System

The integration constants can be determined by solving the following linear equations (i.e., Cramer's system) which can be written in matrix form as [65]

$$[IC] = [BC]^{-1} \cdot [ES], \tag{37}$$

where $[IC]$ is the integration constants vector (of dimension $X_{\max} \times 1$),

$$[IC] = \begin{bmatrix} [IC1] & [IC2] & [IC3] & [IC4] & [IC5] & [IC6] & [IC7] \end{bmatrix}^T, \tag{38a}$$

$$[IC1] = [d1_{h1}^x], \tag{38b}$$

$$[IC2] = [c2_{h2}^x], \tag{38c}$$

$$[IC3] = \begin{bmatrix} c3_{h3}^x & d3_{h3}^x & f3_{n3}^y \end{bmatrix}, \tag{38d}$$

$$[IC4] = \begin{bmatrix} c4_{h4}^x & d4_{h4}^x & e4_{n4}^y \end{bmatrix}, \tag{38e}$$

$$[IC5] = \begin{bmatrix} c5_{h5}^x & d5_{h5}^x & e5_{n5}^y & f5_{n5}^y \end{bmatrix}, \tag{38f}$$

$$[IC6] = \begin{bmatrix} c6_0^x & c6_{h6}^x & d6_0^x & d6_{h6}^x & e6_{n6}^y & f6_{n6}^y \end{bmatrix}, \tag{38g}$$

$$[IC7] = \begin{bmatrix} c7_0^x & c7_{h7}^x & d7_0^x & d7_{h7}^x & e7_{n7}^y & f7_{n7}^y \end{bmatrix}, \tag{38h}$$

Preprints (www.preprints.org) | NOT PEER-REVIEWED | Posted: 27 September 2016 doi:10.20944/preprints201609.0106.v1

$[ES]$ the electromagnetic sources vector (of dimension $X_{\max} \times 1$),

$$[ES] = \begin{bmatrix} [ES1] & [ES2] & [ES3] & [ES4] & [ES5] & [ES6] & [ES7] \end{bmatrix}^T, \tag{39a}$$

$$[ES1] = [ES16_{h1} + ES17_{h1}], \tag{39b}$$

$$[ES2] = [ES26_{h2} + ES27_{h2}], \tag{39c}$$

$$[ES3] = \begin{bmatrix} 0 & 0 & ES36_{n3} \end{bmatrix}, \tag{39d}$$

$$[ES4] = \begin{bmatrix} 0 & 0 & ES47_{n4} \end{bmatrix}, \tag{39e}$$

$$[ES5] = \begin{bmatrix} 0 & 0 & ES56_{n5} & ES57_{n5} \end{bmatrix}, \tag{39f}$$

$$[ES6] = \begin{bmatrix} ES61_0 & 0 & ES62_0 & 0 & 0 & 0 \end{bmatrix}, \tag{39g}$$

$$[ES7] = \begin{bmatrix} ES71_0 & 0 & ES72_0 & 0 & 0 & 0 \end{bmatrix}, \tag{39h}$$

and $[BC]$ the boundary conditions matrix (of dimension $X_{\max} \times X_{\max}$)

$$[BC] = \begin{bmatrix} [I] & 0 & [BC13] & [BC14] & [BC15] & [BC16] & [BC17] \\ 0 & [I] & [BC23] & [BC24] & [BC25] & [BC26] & [BC27] \\ [BC31] & [BC32] & [I] & 0 & 0 & [BC36] & 0 \\ [BC41] & [BC42] & 0 & [I] & 0 & 0 & [BC47] \\ [BC51] & [BC52] & 0 & 0 & [I] & [BC56] & [BC57] \\ [BC61] & [BC62] & [BC63] & 0 & [BC65] & [I] & 0 \\ [BC71] & [BC72] & 0 & [BC74] & [BC75] & 0 & [I] \end{bmatrix}, \tag{40a}$$

in which $[I]$ is identity matrix, and

$$\begin{aligned} [BC13] &= \begin{bmatrix} Q13c_{h1,h3} & Q13d_{h1,h3} & Q13f_{h1,n3} \end{bmatrix} \\ [BC14] &= \begin{bmatrix} Q14c_{h1,h4} & Q14d_{h1,h4} & Q14e_{h1,n4} \end{bmatrix} \\ [BC15] &= \begin{bmatrix} Q15c_{h1,h5} & Q15d_{h1,h5} & Q15e_{h1,n5} & Q15f_{h1,n5} \end{bmatrix} \\ [BC16] &= \begin{bmatrix} Q16c_{h1,0} & Q16c_{h1,h6} & Q16d_{h1,0} & Q16d_{h1,h6} & Q16e_{h1,n6} & Q16f_{h1,n6} \end{bmatrix} \\ [BC17] &= \begin{bmatrix} Q17c_{h1,0} & Q17c_{h1,h7} & Q17d_{h1,0} & Q17d_{h1,h7} & Q17e_{h1,n7} & Q17f_{h1,n7} \end{bmatrix} \end{aligned} \tag{40b}$$

for Region 1,

$$\begin{aligned} [BC23] &= \begin{bmatrix} Q23c_{h2,h3} & Q23d_{h2,h3} & Q23f_{h2,n3} \end{bmatrix} \\ [BC24] &= \begin{bmatrix} Q24c_{h2,h4} & Q24d_{h2,h4} & Q24e_{h2,n4} \end{bmatrix} \\ [BC25] &= \begin{bmatrix} Q25c_{h2,h5} & Q25d_{h2,h5} & Q25e_{h2,n5} & Q25f_{h2,n5} \end{bmatrix} \\ [BC26] &= \begin{bmatrix} Q26c_{h2,0} & Q26c_{h2,h6} & Q26d_{h2,0} & Q26d_{h2,h6} & Q26e_{h2,n6} & Q26f_{h2,n6} \end{bmatrix} \\ [BC27] &= \begin{bmatrix} Q27c_{h2,0} & Q27c_{h2,h7} & Q27d_{h2,0} & Q27d_{h2,h7} & Q27e_{h2,n7} & Q27f_{h2,n7} \end{bmatrix} \end{aligned} \tag{40c}$$

Preprints (www.preprints.org) | NOT PEER-REVIEWED | Posted: 27 September 2016 doi:10.20944/preprints201609.0106.v1

for Region 2,

$$
\begin{aligned}
[BC31] &= \begin{bmatrix} Q31d_{h3,h1} & 0 & 0 \end{bmatrix}^T \\
[BC32] &= \begin{bmatrix} 0 & Q32c_{h3,h2} & 0 \end{bmatrix}^T \\
[BC36] &= \begin{bmatrix} 0 & 0 & 0 & 0 & 0 & 0 \\ 0 & 0 & 0 & 0 & 0 & 0 \\ Q36c_{n3,0} & Q36c_{n3,h6} & Q36d_{n3,0} & Q36d_{n3,h6} & Q36e_{n3,n6} & Q36f_{n3,n6} \end{bmatrix}
\end{aligned} \tag{40d}
$$

for Region 3,

$$
\begin{aligned}
[BC41] &= \begin{bmatrix} Q41d_{h4,h1} & 0 & 0 \end{bmatrix}^T \\
[BC42] &= \begin{bmatrix} 0 & Q42c_{h4,h2} & 0 \end{bmatrix}^T \\
[BC47] &= \begin{bmatrix} 0 & 0 & 0 & 0 & 0 & 0 \\ 0 & 0 & 0 & 0 & 0 & 0 \\ Q47c_{n4,0} & Q47c_{n4,h7} & Q47d_{n4,0} & Q47d_{n4,h7} & Q47e_{n4,n7} & Q47f_{n4,n7} \end{bmatrix}
\end{aligned} \tag{40e}
$$

for Region 4,

$$
\begin{aligned}
[BC51] &= \begin{bmatrix} Q51d_{h5,h1} & 0 & 0 & 0 \end{bmatrix}^T \\
[BC52] &= \begin{bmatrix} 0 & Q52c_{h5,h2} & 0 & 0 \end{bmatrix}^T \\
[BC56] &= \begin{bmatrix} 0 & 0 & 0 & 0 & 0 & 0 \\ 0 & 0 & 0 & 0 & 0 & 0 \\ Q56c_{n5,0} & Q56c_{n5,h6} & Q56d_{n5,0} & Q56d_{n5,h6} & Q56e_{n5,n6} & Q56f_{n5,n6} \\ 0 & 0 & 0 & 0 & 0 & 0 \end{bmatrix} \\
[BC57] &= \begin{bmatrix} 0 & 0 & 0 & 0 & 0 & 0 \\ 0 & 0 & 0 & 0 & 0 & 0 \\ 0 & 0 & 0 & 0 & 0 & 0 \\ Q57c_{n5,0} & Q57c_{n5,h7} & Q57d_{n5,0} & Q57c_{n5,h7} & Q57e_{n5,n7} & Q57f_{n5,n7} \end{bmatrix}
\end{aligned} \tag{40f}
$$

for Region 5,

$$
\begin{aligned}
[BC61] &= \begin{bmatrix} Q61d_{0,h1} & Q61d_{h6,h1} & 0 & 0 & 0 & 0 \end{bmatrix}^T \\
[BC62] &= \begin{bmatrix} 0 & 0 & Q62c_{0,h2} & Q62c_{h6,h2} & 0 & 0 \end{bmatrix}^T \\
[BC63] &= \begin{bmatrix} 0 & 0 & 0 \\ 0 & 0 & 0 \\ 0 & 0 & 0 \\ 0 & 0 & 0 \\ 0 & 0 & 0 \\ Q63c_{n6,h3} & Q63d_{n6,h3} & Q63f_{n6,n3} \end{bmatrix} \\
[BC65] &= \begin{bmatrix} 0 & 0 & 0 & 0 \\ 0 & 0 & 0 & 0 \\ 0 & 0 & 0 & 0 \\ 0 & 0 & 0 & 0 \\ Q65c_{n6,h5} & Q65d_{n6,h5} & Q65e_{n6,n5} & Q65f_{n6,n5} \\ 0 & 0 & 0 & 0 \end{bmatrix}
\end{aligned} \tag{40g}
$$

Preprints (www.preprints.org) | NOT PEER-REVIEWED | Posted: 27 September 2016 doi:10.20944/preprints201609.0106.v1

for Region 6,

$$
\begin{aligned}
[BC71] &= \begin{bmatrix} Q71d_{0,h1} & Q71d_{h7,h1} & 0 & 0 & 0 & 0 \end{bmatrix}^T \\
[BC72] &= \begin{bmatrix} 0 & 0 & Q72c_{0,h2} & Q72c_{h7,h2} & 0 & 0 \end{bmatrix}^T \\
[BC74] &= \begin{bmatrix} 0 & 0 & 0 \\ 0 & 0 & 0 \\ 0 & 0 & 0 \\ 0 & 0 & 0 \\ Q74c_{n7,h4} & Q74d_{n7,h4} & Q74e_{n7,n4} \\ 0 & 0 & 0 \end{bmatrix} \\
[BC75] &= \begin{bmatrix} 0 & 0 & 0 & 0 \\ 0 & 0 & 0 & 0 \\ 0 & 0 & 0 & 0 \\ 0 & 0 & 0 & 0 \\ 0 & 0 & 0 & 0 \\ Q75c_{n7,h5} & Q75d_{n7,h5} & Q75e_{n7,n5} & Q75f_{n7,n5} \end{bmatrix}
\end{aligned}
\tag{40h}
$$

for Region 7.

The corresponding elements in (39) and (40) are defined in the **Appendix C**. One can note that (37) consists of

$$
X_{\max} = \begin{bmatrix} H1_{\max} + H2_{\max} + 2 \cdot H3_{\max} + N3_{\max} + 2 \cdot H4_{\max} + N4_{\max} \\ \cdots + 2 \cdot (H5_{\max} + N5_{\max}) + 2 \cdot (H6_{\max} + N6_{\max} + 1) + 2 \cdot (H7_{\max} + N7_{\max} + 1) \end{bmatrix} \tag{41}
$$

equations and unknowns. Any mathematical software (such as Matlab® or Mathcad® for example) can quickly give the numerical solution of (37). The analytical solutions of the magnetic flux density in the various regions have been computed with a finite number of spatial harmonics terms $H1_{max}$ - $H7_{max}$ (for the x-edges) and $N3_{max}$ - $N7_{max}$ (for the y-edges) as indicated in Table 1.

Table 1. Parameters of the Air- or Iron-Core Coil.

Parameters, Symbols, Units	Values
Number of series turns, N_t [-]	1,600
Maximum direct current, I [A]	5
Surface of conductors, S_c [mm^2]	800
Current density (due to supply currents), J_{zk} [A/mm^2]	$\pm$ 10
Effective axial length, L_z [cm]	4
Geometrical parameters in the x-axis, $\{x_1; x_2; x_3; x_4; x_5; x_6\}$ [cm]	$\{0; 10; 12; 16; 18; 28\}$
Geometrical parameters in the y-axis, $\{y_1; y_2; y_3; y_4\}$ [cm]	$\{0; 10; 14; 24\}$
Relative magnetic permeability of the iron, μ_{iron} [-]	1,500
Number of spatial harmonics for Region 1, $H1_{max}$ [-]	98
Number of spatial harmonics for Region 2, $H2_{max}$ [-]	98
Number of spatial harmonics for Region 3, $\{H3_{\max};\ N3_{\max}\}$ [-]	$\{35; 88\}$
Number of spatial harmonics for Region 4, $\{H4_{\max};\ N4_{\max}\}$ [-]	$\{35; 88\}$
Number of spatial harmonics for Region 5, $\{H5_{\max};\ N5_{\max}\}$ [-]	$\{14; 88\}$
Number of spatial harmonics for Region 6, $\{H6_{\max};\ N6_{\max}\}$ [-]	$\{7; 88\}$
Number of spatial harmonics for Region 7, $\{H7_{\max};\ N7_{\max}\}$ [-]	$\{7; 88\}$

Preprints (www.preprints.org) | NOT PEER-REVIEWED | Posted: 27 September 2016 doi:10.20944/preprints201609.0106.v1

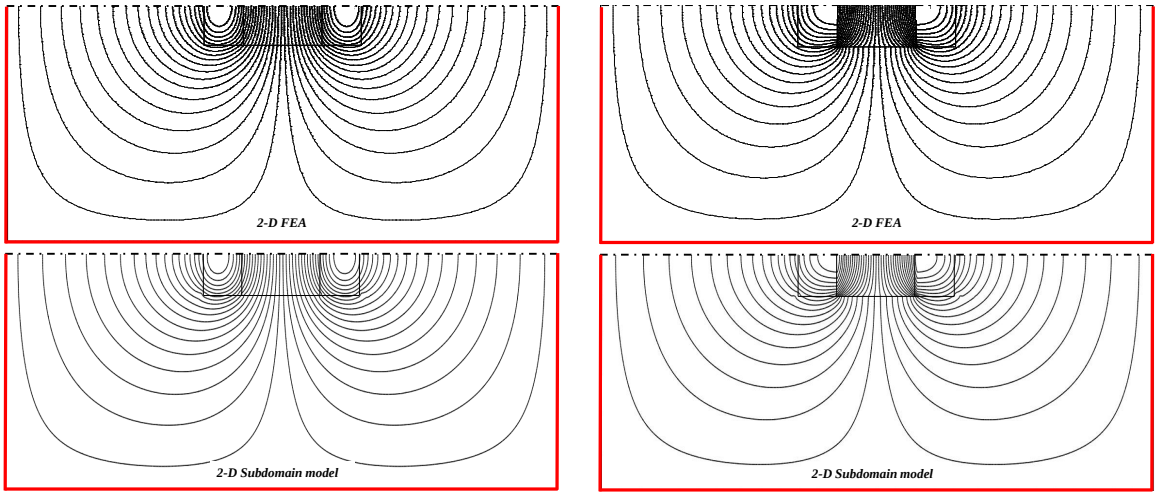

Figure 5. Equipotential lines of A_z with the 2-D subdomain model and FEA for **(a)** air- and **(b)** iron-core coil.

3. Comparison of the Semi-Analytic and Finite-Element Calculations

3.1. Introduction

The objective of this section is to show the effectiveness of 2-D subdomain model on the magnetic field distribution. The main parameters of the air- and iron-cored coil are given in Table 1. For the comparison, the system has been set up using Cedrat's Flux2D software package (i.e., an advanced finite-element method based numeric field analysis program) [8]. The finite-element computations are done under same assumptions on which the semi-analytical model is based [see § 2.1. Problem Description and Assumptions]. The Cramer's system (37) consists of 1,100 elements which is much smaller than the 2-D FEA mesh having 8,566 surfaces elements of second order. The personal computer used for this comparison has the following characteristics: HP Z800 Intel(R) Xeon(R) CPU@2.4 GHz (with 2 processors) RAM 16 Go 64 bits.

3.2. Results Discussion

The 2-D subdomain model is implemented so that it is possible to get values of A_z in the air- and iron-core coil. Figure 5 present the equipotential lines ($\approx$ 30 lines) of A_z in the system with the semi-analytical model and FEA. As can be seen, a good evaluation is obtained, comparing those results with 2-D FEA, for both air- and iron-core.

The paths of the magnetic flux density validation for the comparison are given in Figure 6. The waveforms of the components of $\overrightarrow{B} = \{B_x; B_y; 0\}$ are represented on the various paths in Figure 7 - Figure 11. The solid lines represent the magnetic flux density computed by the 2-D FEA and the circles correspond to 2-D subdomain model. It can be seen that a very good agreement is obtained for the components of $\overrightarrow{B}$, whatever the paths, for both air- and iron-core. This confirms that the saturation effect, with a constant magnetic permeability corresponding to linear zone of $B(H)$ curve, is taken into account accurately. It is interesting to note that numerical peaks appear in the FEA results [see Figure 8a and Figure 11a] which are mainly due to the mesh. Some slight discrepancies are observed between numerical and analytical results which can be caused by the finite number of spatial harmonic taken into account in the semi-analytical model according to the x- and y-edges. The increase of harmonics number can resolve these deviations, however, at the expense of the computation time.

Preprints (www.preprints.org) | NOT PEER-REVIEWED | Posted: 27 September 2016 doi:10.20944/preprints201609.0106.v1

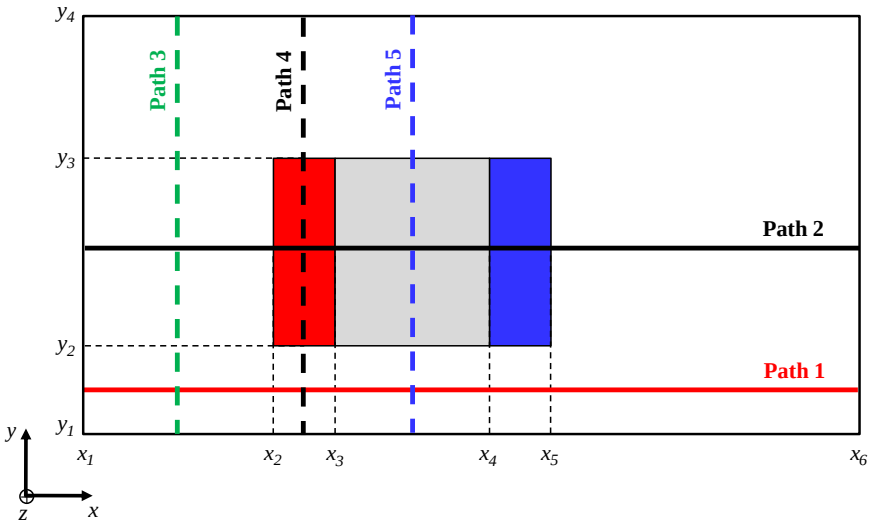

Figure 6. Paths of the magnetic flux density validation for the comparison.

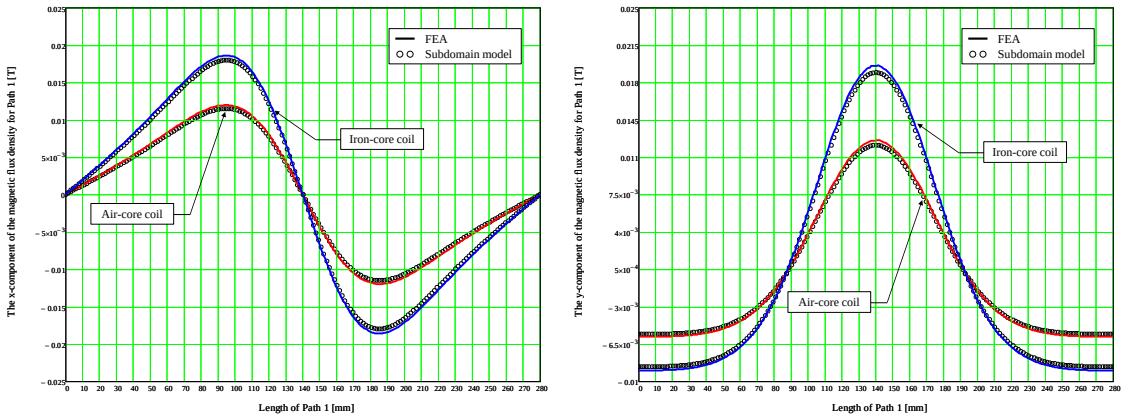

(a) **(b)**

Figure 7. Waveform of the **(a)** x- and **(b)** y-components for Path 1.

4. Conclusion

An overview on the existing (semi-)analytical models in Maxwell-Fourier methods (i.e., multi-layers models and subdomain technique) with the saturation effect has been realized. It has been demonstrated that there is no (semi-)analytical model based on the subdomain technique taking into account the iron parts with(out) the nonlinear $B(H)$ curve. Then, the new scientific contribution on the 2-D subdomain technique in Cartesian coordinates to study the local magnetic field distribution in the iron parts is presented in this paper.

It was performed by solving 2-D magnetostatic Maxwell's equations in Cartesian coordinates (x, y) for an air- or iron-core coil supplied by a direct current. The subdomains connection is carried out in the two directions (i.e., x- and y-edges). The iron magnetic permeability is constant corresponding to linear zone of the initial magnetization curve. However, nonlinear magnetic materials could be accounted for by means of an iterative algorithm. This major scientific contribution will be applied to rotating and/or linear electrical machines with(out) magnets supplied by a direct current or alternate current (with any waveforms) whose the analysis would be based on a 2-D semi-analytical model in Cartesian coordinates (e.g., plane linear machines, axial-flux machines,...).

Preprints (www.preprints.org) | NOT PEER-REVIEWED | Posted: 27 September 2016 doi:10.20944/preprints201609.0106.v1

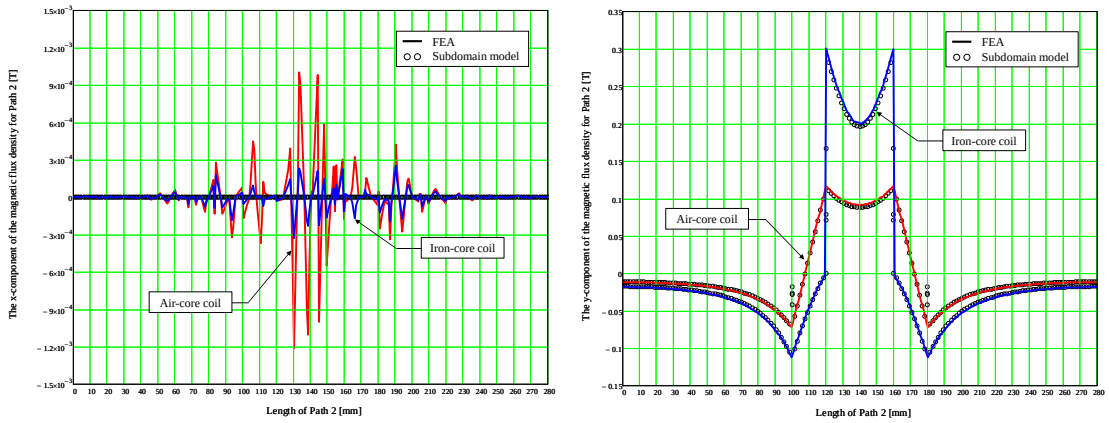

(a) **(b)**

Figure 8. Waveform of the **(a)** x- and **(b)** y-components for Path 2.

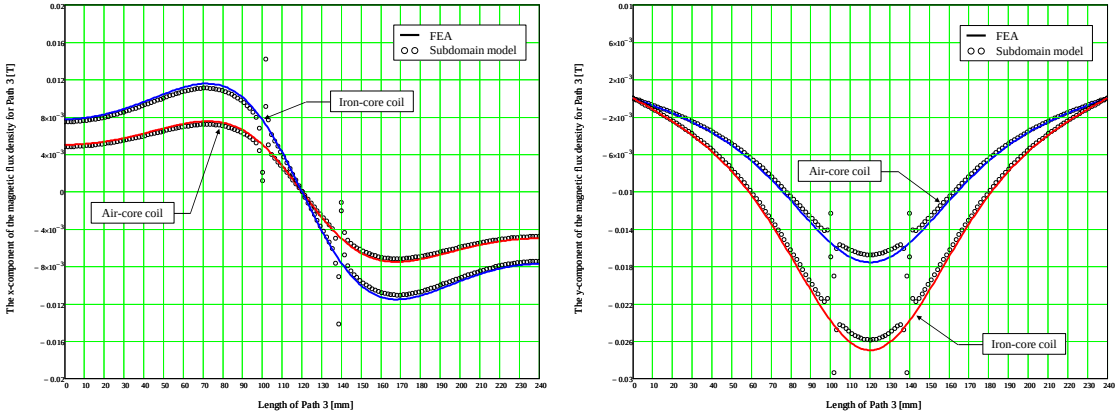

(a) **(b)**

Figure 9. Waveform of the **(a)** x- and **(b)** y-components for Path 3.

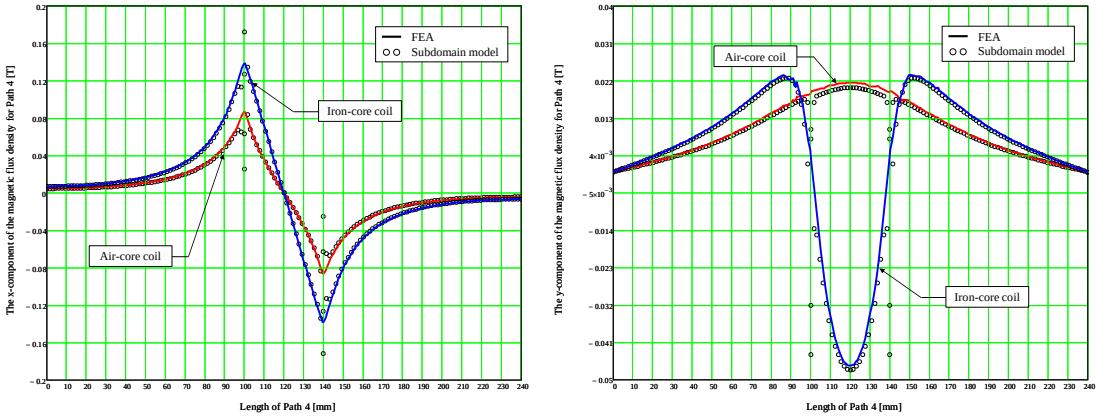

(a) **(b)**

Figure 10. Waveform of the **(a)** x- and **(b)** y-components for Path 4.

Preprints (www.preprints.org) | NOT PEER-REVIEWED | Posted: 27 September 2016 doi:10.20944/preprints201609.0106.v1

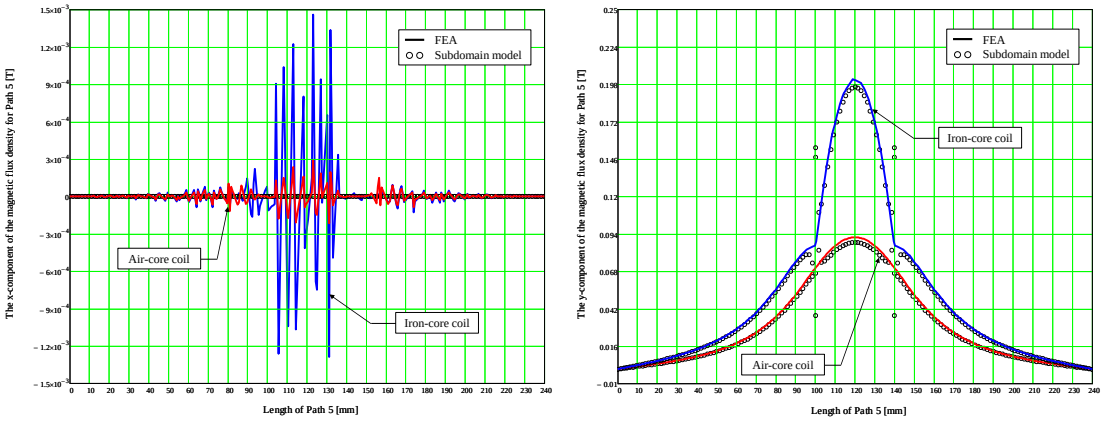

(a) **(b)**

Figure 11. Waveform of the **(a)** x- and **(b)** y-components for Path 5.

An extension of the 2-D subdomain technique in polar coordinates as well as various electrical machines (viz., radial-/axial-/transverse-flux machines, linear machines, U-/E-cored electromagnet device,...) will be made in the next studies.

This new approach to account for the saturation effect is (semi-)analytically based and takes significantly less computing time than the FEA; it is eminently suitable for design and optimization of the electromechanical systems. Predicted results from the exact (semi-)analytical model have been compared finite-element predictions, and good agreement has been achieved, in both amplitudes and waveforms.

Author Contributions: This paper is the results of the hard work of all authors, which have wrote the paper and have gave advices for the manuscripts.

Conflicts of Interest: The authors declare no conflict of interest.

Appendix A The 2-D Magnetostatic General Solution in Cartesian Coordinates

Appendix A.1 Governing Partial Differential Equations (EDPs)

By assuming that the term $\partial \overrightarrow{D} \Big/ \partial t$ is negligible, the magnetostatic Maxwell's equations are represented by Maxwell-Ampère

$$\overrightarrow{rot\left(\overrightarrow{H}\right)} = \overrightarrow{J} \quad (with\ \overrightarrow{J} = 0\ for\ the\ no\text{-}load\ operation), \tag{A.1a}$$

and Maxwell-Thomson

$$div\left(\overrightarrow{B}\right) = 0 \quad (Magnetic\ flux\ conservation), \tag{A.1b}$$

$$\overrightarrow{B} = \overrightarrow{rot\left(\overrightarrow{A}\right)} \quad \text{with} \quad div\left(\overrightarrow{A}\right) = 0 \quad (Coulomb's\ gauge), \tag{A.1c}$$

where $\overrightarrow{A}$, $\overrightarrow{B}$, $\overrightarrow{H}$, and $\overrightarrow{J}$ are respectively the magnetic vector potential, the magnetic flux density, magnetic field, and the current density (due to supply currents) vectors.

The field vectors $\overrightarrow{B}$ and $\overrightarrow{H}$ are coupled by the magnetic material equation

$$\overrightarrow{B} = \mu \cdot \overrightarrow{H} + \mu_0 \cdot \overrightarrow{M}, \tag{A.2}$$

Preprints (www.preprints.org) | NOT PEER-REVIEWED | Posted: 27 September 2016 doi:10.20944/preprints201609.0106.v1

where $\overrightarrow{M}$ is the magnetization vector (with $\overrightarrow{M} = 0$ for the vacuum/iron or $\overrightarrow{M} \neq 0$ for the magnets according to the magnetization direction [4]), and $\mu = \mu_0 \cdot \mu_r$ the absolute magnetic permeability of the magnetic material in which μ_0 and μ_r are respectively the vacuum permeability and the relative permeability of the magnetic material (with $\mu_r = 1$ for the vacuum or $\mu_r \neq 1$ for the magnets/iron).

By using (A.1) and (A.2), the general EDPs of magnetostatic are defined by [64]:

$$\overrightarrow{X}_A - \nu \cdot \Delta \overrightarrow{A} = \overrightarrow{J} + \overrightarrow{X}_B, \tag{A.3a}$$

$$\overrightarrow{X}_A = \overrightarrow{grad\,(\nu)} \wedge \overrightarrow{rot\left(\overrightarrow{A}\right)}, \tag{A.3b}$$

$$\overrightarrow{X}_B = \mu_0 \cdot \left[\overrightarrow{grad\,(\nu)} \wedge \overrightarrow{M} + \nu \cdot \overrightarrow{rot\left(\overrightarrow{M}\right)}\right], \tag{A.3c}$$

where $\nu = 1/\mu$ is the absolute magnetic reluctivity of the magnetic material.

By neglecting the end-effects (i.e., the system is infinitely long which leads to $\overrightarrow{A} = \{0; 0; A_z\}$: the magnetic variables are independent of z), (A.3) in Cartesian coordinates (x, y) with $\mu = C^{st}$ can be expressed by:

$$\Delta A_z = \frac{\partial^2 A_z}{\partial x^2} + \frac{\partial^2 A_z}{\partial y^2} = ES, \tag{A.4a}$$

$$ES = -\left[\mu \cdot J_z + \mu_0 \cdot \left(\frac{\partial M_y}{\partial x} - \frac{\partial M_x}{\partial y}\right)\right]. \tag{A.4b}$$

Appendix A.2 General Solution

It is interesting to note that A_z is governed by Poisson's equation, when there is one or more electromagnetic sources (i.e., $ES \neq 0$), or Laplace's equation, when there is no electromagnetic sources (i.e., $ES = 0$). According to the method of separation of variables, the 2-D magnetostatic general solution of A_z in Cartesian coordinates (x, y) can be written as

$$A_z = A_z^x + A_z^y + A_{zP}, \tag{A.5a}$$

$$A_z^x = \left| \begin{array}{l} \left(C_0^x + D_0^x \cdot y\right) \cdot \left(E_0^x + F_0^x \cdot x\right) \\ \cdots + \sum_{h=1}^{\infty} \left[\begin{array}{l} C_h^x \cdot \mathrm{ch}\left(\beta_h \cdot y\right) \\ \cdots + D_h^x \cdot \mathrm{sh}\left(\beta_h \cdot y\right) \end{array}\right] \cdot \left[\begin{array}{l} E_h^x \cdot \cos\left(\beta_h \cdot x\right) \\ \cdots + F_h^x \cdot \sin\left(\beta_h \cdot x\right) \end{array}\right] \end{array} \right., \tag{A.5b}$$

$$A_z^y = \left| \begin{array}{l} \left(C_0^y + D_0^y \cdot y\right) \cdot \left(E_0^y + F_0^y \cdot x\right) \\ \cdots + \sum_{n=1}^{\infty} \left[\begin{array}{l} C_n^y \cdot \cos\left(\lambda_n \cdot y\right) \\ \cdots + D_n^y \cdot \sin\left(\lambda_n \cdot y\right) \end{array}\right] \cdot \left[\begin{array}{l} E_n^y \cdot \mathrm{ch}\left(\lambda_n \cdot x\right) \\ \cdots + F_n^y \cdot \mathrm{sh}\left(\lambda_n \cdot x\right) \end{array}\right] \end{array} \right., \tag{A.5c}$$

where A_{zP} are the particular solution of $A_z$respecting the second member ES in (A.4), C_0^x - F_h^x & C_0^y - F_h^y the integration constants, β_h & λ_n the periodicity of A_z^x & A_z^y, and h & n the spatial harmonic orders.

According to (A.1c), the components of $\overrightarrow{B} = \{B_x; B_y; 0\}$ can be deduced from A_z by

$$B_x = \frac{\partial A_z}{\partial y} \quad \text{and} \quad B_y = -\frac{\partial A_z}{\partial x} \tag{A.6}$$

which leads to

$$B_x = B_x^x + B_x^y + \frac{\partial A_{zP}}{\partial y}, \tag{A.7a}$$

$$B_x^x = \left| \begin{array}{l} D_0^x \cdot \left(E_0^x + F_0^x \cdot x\right) \\ \cdots + \sum_{h=1}^{\infty} \beta_h \cdot \left[\begin{array}{l} C_h^x \cdot sh\left(\beta_h \cdot y\right) \\ \cdots + D_h^x \cdot ch\left(\beta_h \cdot y\right) \end{array}\right] \cdot \left[\begin{array}{l} E_h^x \cdot \cos\left(\beta_h \cdot x\right) \\ \cdots + F_h^x \cdot \sin\left(\beta_h \cdot x\right) \end{array}\right] \end{array} \right., \tag{A.7b}$$

Preprints (www.preprints.org) | NOT PEER-REVIEWED | Posted: 27 September 2016 doi:10.20944/preprints201609.0106.v1

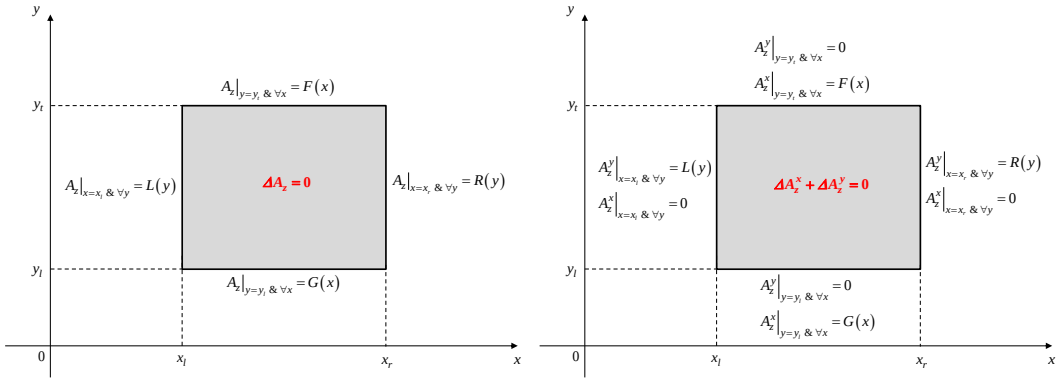

(a) **(b)**

Figure B.1. A_z imposed on all edges of a region: **(a)** General and **(b)** According to the principle of superposition.

$$B_x^y = \left| \begin{array}{l} D_0^y \cdot \left(E_0^y + F_0^y \cdot x\right) \\ \cdots + \sum_{n=1}^{\infty} \lambda_n \cdot \left[\begin{array}{l} -C_n^y \cdot \sin\left(\lambda_n \cdot y\right) \\ \cdots + D_n^y \cdot \cos\left(\lambda_n \cdot y\right) \end{array} \right] \cdot \left[\begin{array}{l} E_n^y \cdot \mathrm{ch}\left(\lambda_n \cdot x\right) \\ \cdots + F_n^y \cdot \mathrm{sh}\left(\lambda_n \cdot x\right) \end{array} \right] \end{array} \right. , \tag{A.7c}$$

and

$$B_y = B_y^x + B_y^y - \frac{\partial A_{zP}}{\partial x}, \tag{A.8a}$$

$$B_y^x = -\left| \begin{array}{l} F_0^x \cdot \left(C_0^x + D_0^x \cdot y\right) \\ \cdots + \sum_{h=1}^{\infty} \beta_h \cdot \left[\begin{array}{l} C_h^x \cdot \mathrm{ch}\left(\beta_h \cdot y\right) \\ \cdots + D_h^x \cdot \mathrm{sh}\left(\beta_h \cdot y\right) \end{array} \right] \cdot \left[\begin{array}{l} -E_h^x \cdot \sin\left(\beta_h \cdot x\right) \\ \cdots + F_h^x \cdot \cos\left(\beta_h \cdot x\right) \end{array} \right] \end{array} \right. , \tag{A.8b}$$

$$B_y^y = -\left| \begin{array}{l} F_0^y \cdot \left(C_0^y + D_0^y \cdot y\right) \\ \cdots + \sum_{n=1}^{\infty} \lambda_n \cdot \left[\begin{array}{l} C_n^y \cdot \cos\left(\lambda_n \cdot y\right) \\ \cdots + D_n^y \cdot \sin\left(\lambda_n \cdot y\right) \end{array} \right] \cdot \left[\begin{array}{l} E_n^y \cdot sh\left(\lambda_n \cdot x\right) \\ \cdots + F_n^y \cdot ch\left(\lambda_n \cdot x\right) \end{array} \right] \end{array} \right. . \tag{A.8c}$$

Appendix B Simplification of Laplace's Equations according to imposed Boundary Conditions

Appendix B.1 Case-Study no 1: "A_z imposed on all edges of a region"

Figure B.1a shows a region (for $x \in [x_l, x_r]$ and $y \in [y_l, y_t]$)) whose the magnetic vector potentials are imposed on all edges. By applying the principle of superposition on the magnetic quantities, Figure B.1a is redefined by Figure B.1b.

In the case-study no 1, the magnetic vector potential $A_z = A_z^x + A_z^y$, i.e., (A.5), is redefined by

$$A_z^x = \sum_{h=1}^{\infty} \left\{ \frac{c_h^x}{\beta_h} \cdot \frac{sh\left[\beta_h \cdot (y_t - y)\right]}{\mathrm{sh}\left(\beta_h \cdot \tau_y\right)} + \frac{d_h^x}{\beta_h} \cdot \frac{\mathrm{sh}\left[\beta_h \cdot (y - y_l)\right]}{\mathrm{sh}\left(\beta_h \cdot \tau_y\right)} \right\} \cdot \sin\left[\beta_h \cdot (x - x_l)\right], \tag{B.1a}$$

$$A_z^y = \sum_{n=1}^{\infty} \left\{ \frac{e_n^y}{\lambda_n} \cdot \frac{sh\left[\lambda_n \cdot (x_r - x)\right]}{sh\left(\lambda_n \cdot \tau_x\right)} + \frac{f_n^y}{\lambda_n} \cdot \frac{sh\left[\lambda_n \cdot (x - x_l)\right]}{sh\left(\lambda_n \cdot \tau_x\right)} \right\} \cdot \sin\left[\lambda_n \cdot (y - y_l)\right], \tag{B.1b}$$

the component $B_x = B_x^x + B_x^y$ of $\overrightarrow{B}$, i.e., (A.7), by

$$B_x^x = \sum_{h=1}^{\infty} \left\{ -c_h^x \cdot \frac{ch\left[\beta_h \cdot (y_t - y)\right]}{\mathrm{sh}\left(\beta_h \cdot \tau_y\right)} + d_h^x \cdot \frac{ch\left[\beta_h \cdot (y - y_l)\right]}{\mathrm{sh}\left(\beta_h \cdot \tau_y\right)} \right\} \cdot \sin\left[\beta_h \cdot (x - x_l)\right], \tag{B.2a}$$

Preprints (www.preprints.org) | NOT PEER-REVIEWED | Posted: 27 September 2016 doi:10.20944/preprints201609.0106.v1

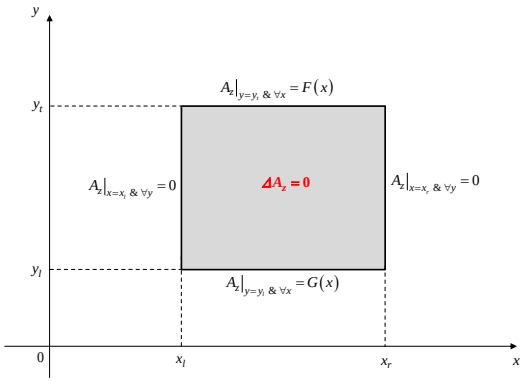

Figure B.2. $A_z = 0$ on x-edges and A_z imposed on y-edges of a region.

$$B_x^y = \sum_{n=1}^{\infty} \left\{ e_n^y \cdot \frac{sh\left[\lambda_n \cdot (x_r - x)\right]}{sh\left(\lambda_n \cdot \tau_x\right)} + f_n^y \cdot \frac{sh\left[\lambda_n \cdot (x - x_l)\right]}{sh\left(\lambda_n \cdot \tau_x\right)} \right\} \cdot \cos\left[\lambda_n \cdot (y - y_l)\right], \tag{B.2b}$$

and the component $B_y = B_y^x + B_y^y$ of $\overrightarrow{B}$, i.e., (A.8), by

$$B_y^x = -\sum_{h=1}^{\infty} \left\{ c_h^x \cdot \frac{sh\left[\beta_h \cdot (y_t - y)\right]}{\mathrm{sh}\left(\beta_h \cdot \tau_y\right)} + d_h^x \cdot \frac{\mathrm{sh}\left[\beta_h \cdot (y - y_l)\right]}{\mathrm{sh}\left(\beta_h \cdot \tau_y\right)} \right\} \cdot \cos\left[\beta_h \cdot (x - x_l)\right], \tag{B.3a}$$

$$B_y^y = -\sum_{n=1}^{\infty} \left\{ -e_n^y \cdot \frac{ch\left[\lambda_n \cdot (x_r - x)\right]}{sh\left(\lambda_n \cdot \tau_x\right)} + f_n^y \cdot \frac{ch\left[\lambda_n \cdot (x - x_l)\right]}{sh\left(\lambda_n \cdot \tau_x\right)} \right\} \cdot \sin\left[\lambda_n \cdot (y - y_l)\right], \tag{B.3b}$$

where c_h^x, d_h^x, e_n^y and f_n^y are new integration constants; $\beta_h = h \cdot \pi/\tau_x$ with $\tau_x = x_r - x_l$; and $\lambda_n = n \cdot \pi/\tau_y$ with $\tau_y = y_t - y_l$.

For the particular case illustrated in Figure B.2 (whose the magnetic vector potentials are zero on x-edges and imposed on y-edges), the magnetic vector potential A_z, according to (B.1) with $A_z^y = 0$, is expressed by

$$A_z = \sum_{h=1}^{\infty} \left\{ \frac{c_h^x}{\beta_h} \cdot \frac{sh\left[\beta_h \cdot (y_t - y)\right]}{\mathrm{sh}\left(\beta_h \cdot \tau_y\right)} + \frac{d_h^x}{\beta_h} \cdot \frac{\mathrm{sh}\left[\beta_h \cdot (y - y_l)\right]}{\mathrm{sh}\left(\beta_h \cdot \tau_y\right)} \right\} \cdot \sin\left[\beta_h \cdot (x - x_l)\right], \tag{B.4a}$$

the x-component of $\overrightarrow{B}$, according to (B.6) with $B_x^y = 0$, by

$$B_x = \sum_{h=1}^{\infty} \left\{ -c_h^x \cdot \frac{ch\left[\beta_h \cdot (y_t - y)\right]}{\mathrm{sh}\left(\beta_h \cdot \tau_y\right)} + d_h^x \cdot \frac{ch\left[\beta_h \cdot (y - y_l)\right]}{\mathrm{sh}\left(\beta_h \cdot \tau_y\right)} \right\} \cdot \sin\left[\beta_h \cdot (x - x_l)\right], \tag{B.4b}$$

the y-component of $\overrightarrow{B}$, according to (B.3) with $B_y^y = 0$, by

$$B_y = -\sum_{h=1}^{\infty} \left\{ c_h^x \cdot \frac{sh\left[\beta_h \cdot (y_t - y)\right]}{\mathrm{sh}\left(\beta_h \cdot \tau_y\right)} + d_h^x \cdot \frac{\mathrm{sh}\left[\beta_h \cdot (y - y_l)\right]}{\mathrm{sh}\left(\beta_h \cdot \tau_y\right)} \right\} \cdot \cos\left[\beta_h \cdot (x - x_l)\right]. \tag{B.4c}$$

Appendix B.2 Case-Study no 2: " B_y and A_z are respectively imposed on x- and y-edges of a region"

Figure B.3a shows a region for $x \in [x_l, x_r]$ and $y \in [y_l, y_t]$)) whose the magnetic flux densities and vector potentials are respectively imposed on x- and y-edges. By applying the principle of superposition on the magnetic quantities, Figure B.3a is redefined by Figure B.3b.

Preprints (www.preprints.org) | NOT PEER-REVIEWED | Posted: 27 September 2016 doi:10.20944/preprints201609.0106.v1

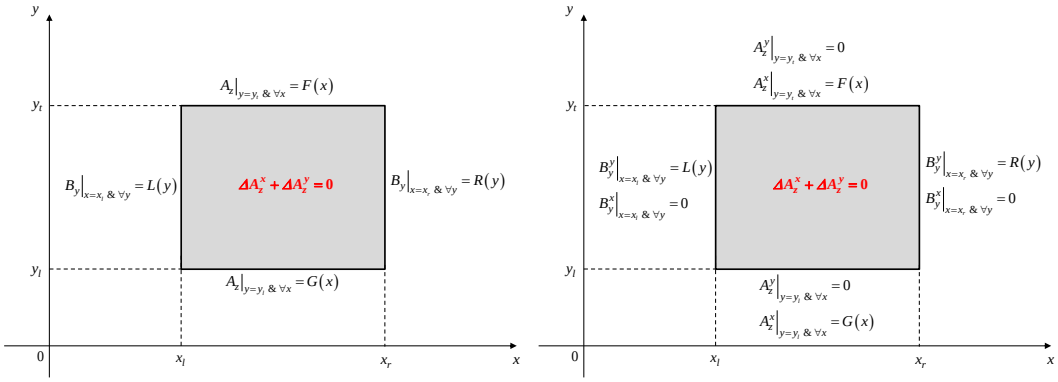

Figure B.3. B_y imposed on x-edges and imposed on y-edges of a region: **(a)** General and **(b)** According to the principle of superposition.

In the case-study no 2, the magnetic vector potential $A_z = A_z^x + A_z^y$, i.e., (A.5), is redefined by

$$A_z^x = \left| \begin{array}{l} (y_t - y) \cdot c_0^x + (y - y_l) \cdot d_0^x \\ \cdots + \sum_{h=1}^{\infty} \left\{ \frac{c_h^x}{\beta_h} \cdot \frac{sh[\beta_h \cdot (y_t - y)]}{\mathrm{sh}(\beta_h \cdot \tau_y)} + \frac{d_h^x}{\beta_h} \cdot \frac{\mathrm{sh}[\beta_h \cdot (y - y_l)]}{\mathrm{sh}(\beta_h \cdot \tau_y)} \right\} \cdot \cos\left[\beta_h \cdot (x - x_l)\right] \end{array} \right. , \tag{B.5a}$$

$$A_z^y = -\sum_{n=1}^{\infty} \left\{ \frac{e_n^y}{\lambda_n} \cdot \frac{\mathrm{ch}\left[\lambda_n \cdot (x - x_l)\right]}{sh\left(\lambda_n \cdot \tau_x\right)} - \frac{f_n^y}{\lambda_n} \cdot \frac{ch\left[\lambda_n \cdot (x_r - x)\right]}{sh\left(\lambda_n \cdot \tau_x\right)} \right\} \cdot \sin\left[\lambda_n \cdot (y - y_l)\right], \tag{B.5b}$$

the component $B_x = B_x^x + B_x^y$ of $\overrightarrow{B}$, i.e., (A.7), by

$$B_x^x = \left| \begin{array}{l} -c_0^x + d_0^x \\ \cdots + \sum_{h=1}^{\infty} \left\{ -c_h^x \cdot \frac{ch[\beta_h \cdot (y_t - y)]}{\mathrm{sh}(\beta_h \cdot \tau_y)} + d_h^x \cdot \frac{ch[\beta_h \cdot (y - y_l)]}{\mathrm{sh}(\beta_h \cdot \tau_y)} \right\} \cdot \cos\left[\beta_h \cdot (x - x_l)\right] \end{array} \right. , \tag{B.6a}$$

$$B_x^y = -\sum_{n=1}^{\infty} \left\{ e_n^y \cdot \frac{\mathrm{ch}\left[\lambda_n \cdot (x - x_l)\right]}{sh\left(\lambda_n \cdot \tau_x\right)} - f_n^y \cdot \frac{ch\left[\lambda_n \cdot (x_r - x)\right]}{sh\left(\lambda_n \cdot \tau_x\right)} \right\} \cdot \cos\left[\lambda_n \cdot (y - y_l)\right], \tag{B.6b}$$

and the component $B_y = B_y^x + B_y^y$ of $\overrightarrow{B}$, i.e., (A.8), by

$$B_y^x = \sum_{h=1}^{\infty} \left\{ c_h^x \cdot \frac{sh\left[\beta_h \cdot (y_t - y)\right]}{\mathrm{sh}\left(\beta_h \cdot \tau_y\right)} + d_h^x \cdot \frac{\mathrm{sh}\left[\beta_h \cdot (y - y_l)\right]}{\mathrm{sh}\left(\beta_h \cdot \tau_y\right)} \right\} \cdot \sin\left[\beta_h \cdot (x - x_l)\right], \tag{B.7a}$$

$$B_y^y = \sum_{n=1}^{\infty} \left\{ e_n^y \cdot \frac{sh\left[\lambda_n \cdot (x - x_l)\right]}{sh\left(\lambda_n \cdot \tau_x\right)} + f_n^y \cdot \frac{sh\left[\lambda_n \cdot (x_r - x)\right]}{sh\left(\lambda_n \cdot \tau_x\right)} \right\} \cdot \sin\left[\lambda_n \cdot (y - y_l)\right], \tag{B.7b}$$

where c_0^x, d_0^x, c_h^x, d_h^x, e_n^y and f_n^y are new integration constants.

Preprints (www.preprints.org) | NOT PEER-REVIEWED | Posted: 27 September 2016 doi:10.20944/preprints201609.0106.v1

Appendix C Elements of Cramer's Systems

Appendix C.1 Simplifying Function of General Integrals

For the determination of the integral constants, it is required to calculate general integrals of the form

$$F_s = \int_{l_l}^{l_l+w} \sin\left[\alpha_s \cdot (l - l_s)\right] \cdot dl, \tag{C.1a}$$

$$F_{cs} = \int_{l_l}^{l_l+w} \cos\left[\alpha_c \cdot (l - l_c)\right] \cdot \sin\left[\alpha_s \cdot (l - l_s)\right] \cdot dl, \tag{C.1b}$$

$$F_{ss} = \int_{l_l}^{l_l+w} \sin\left[\alpha_{s1} \cdot (l - l_{s1})\right] \cdot \sin\left[\alpha_{s2} \cdot (l - l_{s2})\right] \cdot dl, \tag{C.1c}$$

$$F_{ls} = \int_{l_l}^{l_l+w} l \cdot \sin\left[\alpha_s \cdot (l - l_s)\right] \cdot dl, \tag{C.1d}$$

$$F_{l2s} = \int_{l_l}^{l_l+w} l^2 \cdot \sin\left[\alpha_s \cdot (l - l_s)\right] \cdot dl, \tag{C.1e}$$

$$F_{chs} = \int_{l_l}^{l_l+w} ch\left[\alpha_{ch} \cdot (l - l_{ch})\right] \cdot \sin\left[\alpha_s \cdot (l - l_s)\right] \cdot dl, \tag{C.1f}$$

$$F_{shs} = \int_{l_l}^{l_l+w} sh\left[\alpha_{sh} \cdot (l - l_{sh})\right] \cdot \sin\left[\alpha_s \cdot (l - l_s)\right] \cdot dl. \tag{C.1g}$$

The functions (C.1) will be used in the expression of the integration constants. The expressions of (C.1a) - (C.1c) have given in [65]. The development of (C.1d) - (C.1g) gives

$$F_{ls}\left(\alpha_s, l_s, l_l, w\right) = \frac{\left[\begin{array}{l} \sin\left[\alpha_s \cdot (l_l + w - l_s)\right] - \sin\left[\alpha_s \cdot (l_l - l_s)\right] \\ \cdots - \alpha_s \cdot \left\{(l_l + w) \cdot \cos\left[\alpha_s \cdot (l_l + w - l_s)\right] - l_l \cdot \cos\left[\alpha_s \cdot (l_l - l_s)\right]\right\} \end{array}\right]}{\alpha_s^2}, \tag{C.2a}$$

$$F_{l2s}\left(\alpha_s, l_s, l_l, w\right) = \frac{\left[\begin{array}{l} 2 \cdot \left\{\cos\left[\alpha_s \cdot (l_l + w - l_s)\right] - \cos\left[\alpha_s \cdot (l_l - l_s)\right]\right\} \\ \cdots - \alpha_s^2 \cdot \left\{(l_l + w)^2 \cdot \cos\left[\alpha_s \cdot (l_l + w - l_s)\right] - l_l^2 \cdot \cos\left[\alpha_s \cdot (l_l - l_s)\right]\right\} \\ \cdots + 2 \cdot \alpha_s \cdot \left\{(l_l + w) \cdot \sin\left[\alpha_s \cdot (l_l + w - l_s)\right] - l_l \cdot \sin\left[\alpha_s \cdot (l_l - l_s)\right]\right\} \end{array}\right]}{\alpha_s^3}, \tag{C.2b}$$

$$F_{chs}\left(\alpha_{ch}, \alpha_s, l_{ch}, l_s, l_l, w\right) = \frac{\left[\begin{array}{l} -\alpha_{ch} \cdot \left\{\begin{array}{l} sh\left[\alpha_{ch} \cdot (l_l - l_{ch})\right] \cdot \sin\left[\alpha_s \cdot (l_l - l_s)\right] \\ \cdots - sh\left[\alpha_{ch} \cdot (l_l + w - l_{ch})\right] \cdot \sin\left[\alpha_s \cdot (l_l + w - l_s)\right] \end{array}\right\} \\ \cdots + \alpha_s \cdot \left\{\begin{array}{l} ch\left[\alpha_{ch} \cdot (l_l - l_{ch})\right] \cdot \cos\left[\alpha_s \cdot (l_l - l_s)\right] \\ \cdots - ch\left[\alpha_{ch} \cdot (l_l + w - l_{ch})\right] \cdot \cos\left[\alpha_s \cdot (l_l + w - l_s)\right] \end{array}\right\} \end{array}\right]}{\left(\alpha_{ch}^2 + \alpha_s^2\right)}, \tag{C.2c}$$

Preprints (www.preprints.org) | NOT PEER-REVIEWED | Posted: 27 September 2016 doi:10.20944/preprints201609.0106.v1

$$F_{shs}\left(\alpha_{sh},\alpha_s,l_{sh},l_s,l_l,w\right)=\frac{\left[\begin{array}{l}-\alpha_{sh}\cdot\left\{\begin{array}{l}ch\left[\alpha_{sh}\cdot\left(l_l-l_{sh}\right)\right]\cdot\sin\left[\alpha_s\cdot\left(l_l-l_s\right)\right]\\ \cdots-ch\left[\alpha_{sh}\cdot\left(l_l+w-l_{sh}\right)\right]\cdot\sin\left[\alpha_s\cdot\left(l_l+w-l_s\right)\right]\end{array}\right\}\\ \cdots+\alpha_s\cdot\left\{\begin{array}{l}sh\left[\alpha_{sh}\cdot\left(l_l-l_{sh}\right)\right]\cdot\cos\left[\alpha_s\cdot\left(l_l-l_s\right)\right]\\ \cdots-sh\left[\alpha_{sh}\cdot\left(l_l+w-l_{sh}\right)\right]\cdot\cos\left[\alpha_s\cdot\left(l_l+w-l_s\right)\right]\end{array}\right\}\end{array}\right]}{\left(\alpha_{sh}^2+\alpha_s^2\right)}. \tag{C.2d}$$

Appendix C.2 Expression of $d1_{h1}^{x}$ for Region 1

By incorporating $F_1\left(x\right)$ [see Figure 4a] into (7) and by using (13), (18), (23), (28) and (33), the development of (7) gives

$$d1_{h1}^{x}=-\left|\begin{array}{l}\sum_{h3=1}^{\infty}\left(c3_{h3}^{x}\cdot Q13c_{h1,h3}+d3_{h3}^{x}\cdot Q13d_{h1,h3}\right)+\sum_{n3=1}^{\infty}f3_{n3}^{y}\cdot Q13f_{h1,n3}\\ \cdots+\sum_{h4=1}^{\infty}\left(c4_{h4}^{x}\cdot Q14_{h1,h4}+d4_{h4}^{x}\cdot Q14d_{h1,h4}\right)+\sum_{n4=1}^{\infty}e4_{n4}^{y}\cdot Q14e_{h1,n4}\\ \cdots+\sum_{h5=1}^{\infty}\left(c5_{h5}^{x}\cdot Q15c_{h1,h5}+d5_{h5}^{x}\cdot Q15d_{h1,h5}\right)+\sum_{n5=1}^{\infty}\left(e5_{n5}^{y}\cdot Q15e_{h1,n5}+f5_{n5}^{y}\cdot Q15f_{h1,n5}\right)\\ \cdots+\sum_{h6=0}^{\infty}\left(c6_{h6}^{x}\cdot Q16c_{h1,h6}+d6_{h6}^{x}\cdot Q16d_{h1,h6}\right)+\sum_{n6=1}^{\infty}\left(e6_{n6}^{y}\cdot Q16e_{h1,n6}+f6_{n6}^{y}\cdot Q16f_{h1,n6}\right)\\ \cdots+\sum_{h7=0}^{\infty}\left(c7_{h7}^{x}\cdot Q17c_{h1,h7}+d7_{h7}^{x}\cdot Q17d_{h1,h7}\right)+\sum_{n7=1}^{\infty}\left(e7_{n7}^{y}\cdot Q17e_{h1,n7}+f6_{n7}^{y}\cdot Q17f_{h1,n7}\right)\\ \cdots-ES1_{h1}\end{array}\right|, \tag{C.3a}$$

$$Q13c_{h1,h3}=\frac{2}{\tau_{x1}}\cdot\frac{\mu_1}{\mu_3}\cdot\coth\left(\beta_{h3}\cdot\tau_{y3}\right)\cdot F_{ss}\left(\beta3_{h3},\beta1_{h1},x_1,x_1,x_1,\tau_{x3}\right), \tag{C.3b}$$

$$Q13d_{h1,h3}=-\frac{2}{\tau_{x1}}\cdot\frac{\mu_1}{\mu_3}\cdot csch\left(\beta_{h3}\cdot\tau_{y3}\right)\cdot F_{ss}\left(\beta3_{h3},\beta1_{h1},x_1,x_1,x_1,\tau_{x3}\right), \tag{C.3c}$$

$$Q13f_{h1,n3}=-\frac{2}{\tau_{x1}}\cdot\frac{\mu_1}{\mu_3}\cdot csch\left(\lambda_{n3}\cdot\tau_{x3}\right)\cdot F_{shs}\left(\lambda3_{n3},\beta1_{h1},x_1,x_1,x_1,\tau_{x3}\right), \tag{C.3d}$$

$$Q14c_{h1,h4}=\frac{2}{\tau_{x1}}\cdot\frac{\mu_1}{\mu_4}\cdot\coth\left(\beta_{h4}\cdot\tau_{y4}\right)\cdot F_{ss}\left(\beta4_{h4},\beta1_{h1},x_5,x_1,x_5,\tau_{x4}\right), \tag{C.3e}$$

$$Q14d_{h1,h4}=-\frac{2}{\tau_{x1}}\cdot\frac{\mu_1}{\mu_4}\cdot csch\left(\beta_{h4}\cdot\tau_{y4}\right)\cdot F_{ss}\left(\beta4_{h4},\beta1_{h1},x_5,x_1,x_5,\tau_{x4}\right), \tag{C.3f}$$

$$Q14e_{h1,n4}=\frac{2}{\tau_{x1}}\cdot\frac{\mu_1}{\mu_4}\cdot csch\left(\lambda_{n4}\cdot\tau_{x4}\right)\cdot F_{shs}\left(\lambda4_{n4},\beta1_{h1},x_6,x_1,x_5,\tau_{x4}\right), \tag{C.3g}$$

$$Q15c_{h1,h5}=\frac{2}{\tau_{x1}}\cdot\frac{\mu_1}{\mu_5}\cdot\coth\left(\beta_{h5}\cdot\tau_{y5}\right)\cdot F_{ss}\left(\beta5_{h5},\beta1_{h1},x_3,x_1,x_3,\tau_{x5}\right), \tag{C.3h}$$

$$Q15d_{h1,h5}=-\frac{2}{\tau_{x1}}\cdot\frac{\mu_1}{\mu_5}\cdot csch\left(\beta_{h5}\cdot\tau_{y5}\right)\cdot F_{ss}\left(\beta5_{h5},\beta1_{h1},x_3,x_1,x_3,\tau_{x5}\right), \tag{C.3i}$$

$$Q15e_{h1,n5}=\frac{2}{\tau_{x1}}\cdot\frac{\mu_1}{\mu_5}\cdot csch\left(\lambda_{n5}\cdot\tau_{x5}\right)\cdot F_{shs}\left(\lambda5_{n5},\beta1_{h1},x_4,x_1,x_3,\tau_{x5}\right), \tag{C.3j}$$

$$Q15f_{h1,n5}=-\frac{2}{\tau_{x1}}\cdot\frac{\mu_1}{\mu_5}\cdot csch\left(\lambda_{n5}\cdot\tau_{x5}\right)\cdot F_{shs}\left(\lambda5_{n5},\beta1_{h1},x_3,x_1,x_3,\tau_{x5}\right), \tag{C.3k}$$

$$Q16c_{h1,h6}=\frac{2}{\tau_{x1}}\cdot\frac{\mu_1}{\mu_6}\cdot\left\{\begin{array}{ll}F_s\left(\beta1_{h1},x_1,x_2,\tau_{x6}\right) & \text{for } h6=0\\ \coth\left(\beta_{h6}\cdot\tau_{y6}\right)\cdot F_{cs}\left(\beta6_{h6},\beta1_{h1},x_2,x_1,x_2,\tau_{x6}\right) & \text{for } h6\neq0\end{array}\right. \tag{C.3l}$$

$$Q16d_{h1,h6}=-\frac{2}{\tau_{x1}}\cdot\frac{\mu_1}{\mu_6}\cdot\left\{\begin{array}{ll}F_s\left(\beta1_{h1},x_1,x_2,\tau_{x6}\right) & \text{for } h6=0\\ csch\left(\beta_{h6}\cdot\tau_{y6}\right)\cdot F_{cs}\left(\beta6_{h6},\beta1_{h1},x_2,x_1,x_2,\tau_{x6}\right) & \text{for } h6\neq0\end{array}\right. \tag{C.3m}$$

Preprints (www.preprints.org) | NOT PEER-REVIEWED | Posted: 27 September 2016 doi:10.20944/preprints201609.0106.v1

$$Q16e_{h1,n6} = \frac{2}{\tau_{x1}} \cdot \frac{\mu_1}{\mu_6} \cdot csch\left(\lambda_{n6} \cdot \tau_{x6}\right) \cdot F_{chs}\left(\lambda 6_{n6}, \beta 1_{h1}, x_2, x_1, x_2, \tau_{x6}\right), \tag{C.3n}$$

$$Q16f_{h1,n6} = -\frac{2}{\tau_{x1}} \cdot \frac{\mu_1}{\mu_6} \cdot csch\left(\lambda_{n6} \cdot \tau_{x6}\right) \cdot F_{chs}\left(\lambda 6_{n6}, \beta 1_{h1}, x_3, x_1, x_2, \tau_{x6}\right), \tag{C.3o}$$

$$Q17c_{h1,h7} = \frac{2}{\tau_{x1}} \cdot \frac{\mu_1}{\mu_7} \cdot \begin{cases} F_s\left(\beta 1_{h1}, x_1, x_4, \tau_{x7}\right) & \text{for } h7 = 0 \\ \coth\left(\beta_{h7} \cdot \tau_{y7}\right) \cdot F_{cs}\left(\beta 7_{h7}, \beta 1_{h1}, x_4, x_1, x_4, \tau_{x7}\right) & \text{for } h7 \neq 0 \end{cases} \tag{C.3p}$$

$$Q17d_{h1,h7} = -\frac{2}{\tau_{x1}} \cdot \frac{\mu_1}{\mu_7} \cdot \begin{cases} F_s\left(\beta 1_{h1}, x_1, x_4, \tau_{x7}\right) & \text{for } h7 = 0 \\ csch\left(\beta_{h7} \cdot \tau_{y7}\right) \cdot F_{cs}\left(\beta 7_{h7}, \beta 1_{h1}, x_4, x_1, x_4, \tau_{x7}\right) & \text{for } h7 \neq 0 \end{cases} \tag{C.3q}$$

$$Q17e_{h1,n7} = \frac{2}{\tau_{x1}} \cdot \frac{\mu_1}{\mu_7} \cdot csch\left(\lambda_{n7} \cdot \tau_{x7}\right) \cdot F_{chs}\left(\lambda 7_{n7}, \beta 1_{h1}, x_4, x_1, x_4, \tau_{x7}\right), \tag{C.3r}$$

$$Q17f_{h1,n7} = -\frac{2}{\tau_{x1}} \cdot \frac{\mu_1}{\mu_7} \cdot csch\left(\lambda_{n7} \cdot \tau_{x7}\right) \cdot F_{chs}\left(\lambda 7_{n7}, \beta 1_{h1}, x_5, x_1, x_4, \tau_{x7}\right), \tag{C.3s}$$

$$ES16_{h1} = -\mu_1 \cdot \frac{2}{\tau_{x1}} \cdot J_{z6} \cdot y_2 \cdot F_s\left(\beta 1_{h1}, x_1, x_2, \tau_{x6}\right), \tag{C.3t}$$

$$ES17_{h1} = -\mu_1 \cdot \frac{2}{\tau_{x1}} \cdot J_{z7} \cdot y_2 \cdot F_s\left(\beta 1_{h1}, x_1, x_4, \tau_{x7}\right). \tag{C.3u}$$

Appendix C.3 Expression of $c2^x_{h2}$ for Region 2

By incorporating $G_2(x)$ [see Figure 4b] into (11) and by using (13), (18), (23), (28) and (33), the development of (11) gives

$$c2^x_{h2} = -\left| \begin{array}{l} \sum_{h3=1}^{\infty}\left(c3^x_{h3} \cdot Q23c_{h2,h3} + d3^x_{h3} \cdot Q23d_{h2,h3}\right) + \sum_{n3=1}^{\infty} f3^y_{n3} \cdot Q23f_{h2,n3} \\ \cdots + \sum_{h4=1}^{\infty}\left(c4^x_{h4} \cdot Q24c_{h2,h4} + d4^x_{h4} \cdot Q24d_{h2,h4}\right) + \sum_{n4=1}^{\infty} e4^y_{n4} \cdot Q24e_{h2,n4} \\ \cdots + \sum_{h5=1}^{\infty}\left(c5^x_{h5} \cdot Q25c_{h2,h5} + d5^x_{h5} \cdot Q25d_{h2,h5}\right) + \sum_{n5=1}^{\infty}\left(e5^y_{n5} \cdot Q25e_{h2,n5} + f5^y_{n5} \cdot Q25f_{h2,n5}\right) \\ \cdots + \sum_{h6=0}^{\infty}\left(c6^x_{h6} \cdot Q26c_{h2,h6} + d6^x_{h6} \cdot Q26d_{h2,h6}\right) + \sum_{n6=1}^{\infty}\left(e6^y_{n6} \cdot Q26e_{h2,n6} + f6^y_{n6} \cdot Q26f_{h2,n6}\right) \\ \cdots + \sum_{h7=0}^{\infty}\left(c7^x_{h7} \cdot Q27c_{h2,h7} + d7^x_{h7} \cdot Q27d_{h2,h7}\right) + \sum_{n7=1}^{\infty}\left(e7^y_{n7} \cdot Q27e_{h2,n7} + f6^y_{n7} \cdot Q27f_{h2,n7}\right) \\ \cdots - \left(ES26_{h2} + ES27_{h2}\right) \end{array} \right|, \tag{C.4a}$$

$$Q23c_{h2,h3} = \frac{2}{\tau_{x2}} \cdot \frac{\mu_2}{\mu_3} \cdot csch\left(\beta_{h3} \cdot \tau_{y3}\right) \cdot F_{ss}\left(\beta 3_{h3}, \beta 2_{h2}, x_1, x_1, x_1, \tau_{x3}\right), \tag{C.4b}$$

$$Q23d_{h2,h3} = -\frac{2}{\tau_{x2}} \cdot \frac{\mu_2}{\mu_3} \cdot \coth\left(\beta_{h3} \cdot \tau_{y3}\right) \cdot F_{ss}\left(\beta 3_{h3}, \beta 2_{h2}, x_1, x_1, x_1, \tau_{x3}\right), \tag{C.4c}$$

$$Q23f_{h2,n3} = -\frac{2}{\tau_{x2}} \cdot \frac{\mu_2}{\mu_3} \cdot \frac{\cos\left(\lambda_{n3} \cdot \tau_{y3}\right)}{sh\left(\lambda_{n3} \cdot \tau_{x3}\right)} \cdot F_{shs}\left(\lambda 3_{n3}, \beta 2_{h2}, x_1, x_1, x_1, \tau_{x3}\right), \tag{C.4d}$$

$$Q24c_{h2,h4} = \frac{2}{\tau_{x2}} \cdot \frac{\mu_2}{\mu_4} \cdot csch\left(\beta_{h4} \cdot \tau_{y4}\right) \cdot F_{ss}\left(\beta 4_{h4}, \beta 2_{h2}, x_5, x_1, x_5, \tau_{x4}\right), \tag{C.4e}$$

$$Q24d_{h2,h4} = -\frac{2}{\tau_{x2}} \cdot \frac{\mu_2}{\mu_4} \cdot \coth\left(\beta_{h4} \cdot \tau_{y4}\right) \cdot F_{ss}\left(\beta 4_{h4}, \beta 2_{h2}, x_5, x_1, x_5, \tau_{x4}\right), \tag{C.4f}$$

$$Q24e_{h2,n4} = \frac{2}{\tau_{x2}} \cdot \frac{\mu_2}{\mu_4} \cdot \frac{\cos\left(\lambda_{n4} \cdot \tau_{y4}\right)}{sh\left(\lambda_{n4} \cdot \tau_{x4}\right)} \cdot F_{shs}\left(\lambda 4_{n4}, \beta 2_{h2}, x_6, x_1, x_5, \tau_{x4}\right), \tag{C.4g}$$

$$Q25c_{h2,h5} = \frac{2}{\tau_{x2}} \cdot \frac{\mu_2}{\mu_5} \cdot csch\left(\beta_{h5} \cdot \tau_{y5}\right) \cdot F_{ss}\left(\beta 5_{h5}, \beta 2_{h2}, x_3, x_1, x_3, \tau_{x5}\right), \tag{C.4h}$$

Preprints (www.preprints.org) | NOT PEER-REVIEWED | Posted: 27 September 2016 doi:10.20944/preprints201609.0106.v1

$$Q25d_{h2,h5} = -\frac{2}{\tau_{x2}} \cdot \frac{\mu_2}{\mu_5} \cdot \coth\left(\beta_{h5} \cdot \tau_{y5}\right) \cdot F_{ss}\left(\beta 5_{h5}, \beta 2_{h2}, x_3, x_1, x_3, \tau_{x5}\right), \tag{C.4i}$$

$$Q25e_{h2,n5} = \frac{2}{\tau_{x2}} \cdot \frac{\mu_2}{\mu_5} \cdot \frac{\cos\left(\lambda_{n5} \cdot \tau_{y5}\right)}{sh\left(\lambda_{n5} \cdot \tau_{x5}\right)} \cdot F_{shs}\left(\lambda 5_{n5}, \beta 2_{h2}, x_4, x_1, x_3, \tau_{x5}\right), \tag{C.4j}$$

$$Q25f_{h2,n5} = -\frac{2}{\tau_{x2}} \cdot \frac{\mu_2}{\mu_5} \cdot \frac{\cos\left(\lambda_{n5} \cdot \tau_{y5}\right)}{sh\left(\lambda_{n5} \cdot \tau_{x5}\right)} \cdot F_{shs}\left(\lambda 5_{n5}, \beta 2_{h2}, x_3, x_1, x_3, \tau_{x5}\right), \tag{C.4k}$$

$$Q26c_{h2,h6} = \frac{2}{\tau_{x2}} \cdot \frac{\mu_2}{\mu_6} \cdot \begin{cases} F_s\left(\beta 2_{h2}, x_1, x_2, \tau_{x6}\right) & \text{for } h6 = 0 \\ csch\left(\beta_{h6} \cdot \tau_{y6}\right) \cdot F_{cs}\left(\beta 6_{h6}, \beta 2_{h2}, x_2, x_1, x_2, \tau_{x6}\right) & \text{for } h6 \neq 0 \end{cases} \tag{C.4l}$$

$$Q26d_{h2,h6} = -\frac{2}{\tau_{x2}} \cdot \frac{\mu_2}{\mu_6} \cdot \begin{cases} F_s\left(\beta 2_{h2}, x_1, x_2, \tau_{x6}\right) & \text{for } h6 = 0 \\ \coth\left(\beta_{h6} \cdot \tau_{y6}\right) \cdot F_{cs}\left(\beta 6_{h6}, \beta 2_{h2}, x_2, x_1, x_2, \tau_{x6}\right) & \text{for } h6 \neq 0 \end{cases} \tag{C.4m}$$

$$Q26e_{h2,n6} = \frac{2}{\tau_{x2}} \cdot \frac{\mu_2}{\mu_6} \cdot \frac{\cos\left(\lambda_{n6} \cdot \tau_{y6}\right)}{sh\left(\lambda_{n6} \cdot \tau_{x6}\right)} \cdot F_{chs}\left(\lambda 6_{n6}, \beta 2_{h2}, x_2, x_1, x_2, \tau_{x6}\right), \tag{C.4n}$$

$$Q26f_{h2,n6} = -\frac{2}{\tau_{x2}} \cdot \frac{\mu_2}{\mu_6} \cdot \frac{\cos\left(\lambda_{n6} \cdot \tau_{y6}\right)}{sh\left(\lambda_{n6} \cdot \tau_{x6}\right)} \cdot F_{chs}\left(\lambda 6_{n6}, \beta 2_{h2}, x_3, x_1, x_2, \tau_{x6}\right), \tag{C.4o}$$

$$Q27c_{h2,h7} = \frac{2}{\tau_{x2}} \cdot \frac{\mu_2}{\mu_7} \cdot \begin{cases} F_s\left(\beta 2_{h2}, x_1, x_4, \tau_{x7}\right) & \text{for } h7 = 0 \\ csch\left(\beta_{h7} \cdot \tau_{y7}\right) \cdot F_{cs}\left(\beta 7_{h7}, \beta 2_{h2}, x_4, x_1, x_4, \tau_{x7}\right) & \text{for } h7 \neq 0 \end{cases} \tag{C.4p}$$

$$Q27d_{h2,h7} = -\frac{2}{\tau_{x2}} \cdot \frac{\mu_2}{\mu_7} \cdot \begin{cases} F_s\left(\beta 2_{h2}, x_1, x_4, \tau_{x7}\right) & \text{for } h7 = 0 \\ \coth\left(\beta_{h7} \cdot \tau_{y7}\right) \cdot F_{cs}\left(\beta 7_{h7}, \beta 2_{h2}, x_4, x_1, x_4, \tau_{x7}\right) & \text{for } h7 \neq 0 \end{cases} \tag{C.4q}$$

$$Q27e_{h2,n7} = \frac{2}{\tau_{x2}} \cdot \frac{\mu_2}{\mu_7} \cdot \frac{\cos\left(\lambda_{n7} \cdot \tau_{y7}\right)}{sh\left(\lambda_{n7} \cdot \tau_{x7}\right)} \cdot F_{chs}\left(\lambda 7_{n7}, \beta 2_{h2}, x_4, x_1, x_4, \tau_{x7}\right), \tag{C.4r}$$

$$Q27f_{h2,n7} = -\frac{2}{\tau_{x2}} \cdot \frac{\mu_2}{\mu_7} \cdot \frac{\cos\left(\lambda_{n7} \cdot \tau_{y7}\right)}{sh\left(\lambda_{n7} \cdot \tau_{x7}\right)} \cdot F_{chs}\left(\lambda 7_{n7}, \beta 2_{h2}, x_5, x_1, x_4, \tau_{x7}\right), \tag{C.4s}$$

$$ES26_{h2} = -\mu_2 \cdot \frac{2}{\tau_{x2}} \cdot J_{z6} \cdot y_3 \cdot F_s\left(\beta 2_{h2}, x_1, x_2, \tau_{x6}\right), \tag{C.4t}$$

$$ES27_{h2} = -\mu_2 \cdot \frac{2}{\tau_{x2}} \cdot J_{z7} \cdot y_3 \cdot F_s\left(\beta 2_{h2}, x_1, x_4, \tau_{x7}\right), \tag{C.4u}$$

Appendix C.4 Expression of $c3^x_{h3}$, $d3^x_{h3}$ and $f3^y_{n3}$ for Region 3

By using (4), the development of (15a) gives

$$c3^x_{h3} = -\sum_{h1=1}^{\infty} d1^x_{h1} \cdot Q31d_{h3,h1}, \tag{C.5a}$$

$$Q31d_{h3,h1} = -\frac{2}{\tau_{x3}} \cdot \frac{\beta_{h3}}{\beta_{h1}} \cdot th\left(\beta_{h1} \cdot \tau_{y1}\right) \cdot F_{ss}\left(\beta 1_{h1}, \beta 3_{h3}, x_1, x_1, x_1, \tau_{x3}\right). \tag{C.5b}$$

By using (8), the development of (15b) gives

$$d3^x_{h3} = -\sum_{h2=1}^{\infty} c2^x_{h2} \cdot Q32c_{h3,h2}, \tag{C.6a}$$

$$Q32c_{h3,h2} = \frac{2}{\tau_{x3}} \cdot \frac{\beta_{h3}}{\beta_{h2}} \cdot th\left(\beta_{h2} \cdot \tau_{y2}\right) \cdot F_{ss}\left(\beta 2_{h2}, \beta 3_{h3}, x_1, x_1, x_1, \tau_{x3}\right). \tag{C.6b}$$

Preprints (www.preprints.org) | NOT PEER-REVIEWED | Posted: 27 September 2016 doi:10.20944/preprints201609.0106.v1

By using (27), the development of (16) gives

$$f3^{y}_{n3} = -\left| \begin{array}{l} \sum\limits_{h6=0}^{\infty} \left(c6^{x}_{h6} \cdot Q36c_{n3,h6} + d6^{x}_{h6} \cdot Q36d_{n3,h6}\right) \\ \cdots + \sum\limits_{n6=1}^{\infty} \left(e6^{y}_{n6} \cdot Q36e_{n3,n6} + f6^{y}_{n6} \cdot Q36f_{n3,n6}\right) \\ \cdots - ES36_{n3} \end{array} \right. \tag{C.7a}$$

$$Q36c_{n3,h6} = \frac{2}{\tau_{y3}} \cdot \lambda_{n3} \cdot \left\{ \begin{array}{ll} -\left[y_3 \cdot F_s\left(\lambda 3_{n3}, y_2, y_2, \tau_{y3}\right) - F_{ls}\left(\lambda 3_{n3}, y_2, y_2, \tau_{y3}\right)\right] & \text{for } h6 = 0 \\ \frac{1}{\beta_{h6}} \cdot csch\left(\beta_{h6} \cdot \tau_{y6}\right) \cdot F_{shs}\left(\beta 6_{h6}, \lambda 3_{n3}, y_3, y_2, y_2, \tau_{y3}\right) & \text{for } h6 \neq 0 \end{array} \right. \tag{C.7b}$$

$$Q36d_{n3,h6} = \frac{2}{\tau_{y3}} \cdot \lambda_{n3} \cdot \left\{ \begin{array}{ll} \left[y_2 \cdot F_s\left(\lambda 3_{n3}, y_2, y_2, \tau_{y3}\right) - F_{ls}\left(\lambda 3_{n3}, y_2, y_2, \tau_{y3}\right)\right] & \text{for } h6 = 0 \\ \frac{-1}{\beta_{h6}} \cdot csch\left(\beta_{h6} \cdot \tau_{y6}\right) \cdot F_{shs}\left(\beta 6_{h6}, \lambda 3_{n3}, y_2, y_2, y_2, \tau_{y3}\right) & \text{for } h6 \neq 0 \end{array} \right. \tag{C.7c}$$

$$Q36e_{n3,n6} = \frac{2}{\tau_{y3}} \cdot \frac{\lambda_{n3}}{\lambda_{n6}} \cdot csch\left(\lambda_{n6} \cdot \tau_{x6}\right) \cdot F_{ss}\left(\lambda 6_{n6}, \lambda 3_{n3}, y_2, y_2, y_2, \tau_{y3}\right), \tag{C.7d}$$

$$Q36f_{n3,n6} = -\frac{2}{\tau_{y3}} \cdot \frac{\lambda_{n3}}{\lambda_{n6}} \cdot \coth\left(\lambda_{n6} \cdot \tau_{x6}\right) \cdot F_{ss}\left(\lambda 6_{n6}, \lambda 3_{n3}, y_2, y_2, y_2, \tau_{y3}\right), \tag{C.7e}$$

$$ES36_{n3} = -\mu_6 \cdot \frac{\lambda_{n3}}{\tau_{y3}} \cdot J_{z6} \cdot F_{l2s}\left(\lambda 3_{n3}, y_2, y_2, \tau_{y3}\right). \tag{C.7f}$$

Appendix C.5 Expression of $c4^{x}_{h4}$, $d4^{x}_{h4}$ and $e4^{y}_{n4}$ for Region 4

By using (4), the development of (20a) gives

$$c4^{x}_{h4} = -\sum_{h1=1}^{\infty} d1^{x}_{h1} \cdot Q41d_{h4,h1}, \tag{C.8a}$$

$$Q41d_{h4,h1} = -\frac{2}{\tau_{x4}} \cdot \frac{\beta_{h4}}{\beta_{h1}} \cdot th\left(\beta_{h1} \cdot \tau_{y1}\right) \cdot F_{ss}\left(\beta 1_{h1}, \beta 4_{h4}, x_1, x_5, x_5, \tau_{x4}\right). \tag{C.8b}$$

By using (8), the development of (20b) gives

$$d4^{x}_{h4} = -\sum_{h2=1}^{\infty} c2^{x}_{h2} \cdot Q42c_{h4,h2}, \tag{C.9a}$$

$$Q42c_{h4,h2} = \frac{2}{\tau_{x4}} \cdot \frac{\beta_{h4}}{\beta_{h2}} \cdot th\left(\beta_{h2} \cdot \tau_{y2}\right) \cdot F_{ss}\left(\beta 2_{h2}, \beta 4_{h4}, x_1, x_5, x_5, \tau_{x4}\right). \tag{C.9b}$$

By using (32), the development of (21) gives

$$e4^{y}_{n4} = -\left| \begin{array}{l} \sum\limits_{h7=0}^{\infty} \left(c7^{x}_{h7} \cdot Q47c_{n4,h7} + d7^{x}_{h7} \cdot Q47d_{n4,h7}\right) \\ \cdots + \sum\limits_{n7=1}^{\infty} \left(e7^{y}_{n7} \cdot Q47e_{n4,n7} + f7^{y}_{n7} \cdot Q47f_{n4,n7}\right) \\ \cdots - ES47_{n4} \end{array} \right. \tag{C.10a}$$

$$Q47c_{n4,h7} = \frac{2}{\tau_{y4}} \cdot \lambda_{n4} \cdot \left\{ \begin{array}{ll} -\left[y_3 \cdot F_s\left(\lambda 4_{n4}, y_2, y_2, \tau_{y4}\right) - F_{ls}\left(\lambda 4_{n4}, y_2, y_2, \tau_{y4}\right)\right] & \text{for } h7 = 0 \\ \frac{1}{\beta_{h7}} \cdot \frac{\cos\left(\beta_{h7} \cdot \tau_{x7}\right)}{\mathrm{sh}\left(\beta_{h7} \cdot \tau_{y7}\right)} \cdot F_{shs}\left(\beta 7_{h7}, \lambda 4_{n4}, y_3, y_2, y_2, \tau_{y4}\right) & \text{for } h7 \neq 0 \end{array} \right. \tag{C.10b}$$

$$Q47d_{n4,h7} = \frac{2}{\tau_{y4}} \cdot \lambda_{n4} \cdot \left\{ \begin{array}{ll} \left[y_2 \cdot F_s\left(\lambda 4_{n4}, y_2, y_2, \tau_{y4}\right) - F_{ls}\left(\lambda 4_{n4}, y_2, y_2, \tau_{y4}\right)\right] & \text{for } h7 = 0 \\ \frac{-1}{\beta_{h7}} \cdot \frac{\cos\left(\beta_{h7} \cdot \tau_{x7}\right)}{\mathrm{sh}\left(\beta_{h7} \cdot \tau_{y7}\right)} \cdot F_{shs}\left(\beta 7_{h7}, \lambda 4_{n4}, y_2, y_2, y_2, \tau_{y4}\right) & \text{for } h7 \neq 0 \end{array} \right. \tag{C.10c}$$

$$Q47e_{n4,n7} = \frac{2}{\tau_{y4}} \cdot \frac{\lambda_{n4}}{\lambda_{n7}} \cdot \coth\left(\lambda_{n7} \cdot \tau_{x7}\right) \cdot F_{ss}\left(\lambda 7_{n7}, \lambda 4_{n4}, y_2, y_2, y_2, \tau_{y4}\right), \tag{C.10d}$$

Preprints (www.preprints.org) | NOT PEER-REVIEWED | Posted: 27 September 2016 doi:10.20944/preprints201609.0106.v1

$$Q47f_{n4,n7} = -\frac{2}{\tau_{y4}} \cdot \frac{\lambda_{n4}}{\lambda_{n7}} \cdot csch\left(\lambda_{n7} \cdot \tau_{x7}\right) \cdot F_{ss}\left(\lambda 7_{n7}, \lambda 4_{n4}, y_2, y_2, y_2, \tau_{y4}\right), \tag{C.10e}$$

$$ES47_{n4} = -\mu_7 \cdot \frac{\lambda_{n4}}{\tau_{y4}} \cdot J_{z7} \cdot F_{l2s}\left(\lambda 4_{n4}, y_2, y_2, \tau_{y4}\right). \tag{C.10f}$$

Appendix C.6 Expression of $c5^x_{h5}$, $d5^x_{h5}$, $e5^y_{n5}$ and $f5^y_{n5}$ for Region 5

By using (4), the development of (25a) gives

$$c5^x_{h5} = -\sum_{h1=1}^{\infty} d1^x_{h1} \cdot Q51d_{h5,h1}, \tag{C.11a}$$

$$Q51d_{h5,h1} = -\frac{2}{\tau_{x5}} \cdot \frac{\beta_{h5}}{\beta_{h1}} \cdot th\left(\beta_{h1} \cdot \tau_{y1}\right) \cdot F_{ss}\left(\beta 1_{h1}, \beta 5_{h5}, x_1, x_3, x_3, \tau_{x5}\right). \tag{C.11b}$$

By using (8), the development of (25b) gives

$$d5^x_{h5} = -\sum_{h2=1}^{\infty} c2^x_{h2} \cdot Q52c_{h5,h2}, \tag{C.12a}$$

$$Q52c_{h5,h2} = \frac{2}{\tau_{x5}} \cdot \frac{\beta_{h5}}{\beta_{h2}} \cdot th\left(\beta_{h2} \cdot \tau_{y2}\right) \cdot F_{ss}\left(\beta 2_{h2}, \beta 5_{h5}, x_1, x_3, x_3, \tau_{x5}\right). \tag{C.12b}$$

By using (27), the development of (26a) gives

$$e5^y_{n5} = -\left| \begin{array}{l} \sum_{h6=0}^{\infty} \left(c6^x_{h6} \cdot Q56c_{n5,h6} + d6^x_{h6} \cdot Q56d_{n5,h6}\right) \\ \cdots + \sum_{n6=1}^{\infty} \left(e6^y_{n6} \cdot Q56e_{n5,n6} + f6^y_{n6} \cdot Q56f_{n5,n6}\right) \\ \cdots - ES56_{n5} \end{array} \right. \tag{C.13a}$$

$$Q56c_{n5,h6} = \frac{2}{\tau_{y5}} \cdot \lambda_{n5} \cdot \left\{ \begin{array}{ll} -\left[y_3 \cdot F_s\left(\lambda 5_{n5}, y_2, y_2, \tau_{y5}\right) - F_{ls}\left(\lambda 5_{n5}, y_2, y_2, \tau_{y5}\right)\right] & \text{for } h6 = 0 \\ \frac{1}{\beta_{h6}} \cdot \frac{\cos(\beta_{h6} \cdot \tau_{x6})}{\mathrm{sh}(\beta_{h6} \cdot \tau_{y6})} \cdot F_{shs}\left(\beta 6_{h6}, \lambda 5_{n5}, y_3, y_2, y_2, \tau_{y5}\right) & \text{for } h6 \neq 0 \end{array} \right. \tag{C.13b}$$

$$Q56d_{n5,h6} = \frac{2}{\tau_{y5}} \cdot \lambda_{n5} \cdot \left\{ \begin{array}{ll} \left[y_2 \cdot F_s\left(\lambda 5_{n5}, y_2, y_2, \tau_{y5}\right) - F_{ls}\left(\lambda 5_{n5}, y_2, y_2, \tau_{y5}\right)\right] & \text{for } h6 = 0 \\ \frac{-1}{\beta_{h6}} \cdot \frac{\cos(\beta_{h6} \cdot \tau_{x6})}{\mathrm{sh}(\beta_{h6} \cdot \tau_{y6})} \cdot F_{shs}\left(\beta 6_{h6}, \lambda 5_{n5}, y_2, y_2, y_2, \tau_{y5}\right) & \text{for } h6 \neq 0 \end{array} \right. \tag{C.13c}$$

$$Q56e_{n5,n6} = \frac{2}{\tau_{y5}} \cdot \frac{\lambda_{n5}}{\lambda_{n6}} \cdot \coth\left(\lambda_{n6} \cdot \tau_{x6}\right) \cdot F_{ss}\left(\lambda 6_{n6}, \lambda 5_{n5}, y_2, y_2, y_2, \tau_{y5}\right), \tag{C.13d}$$

$$Q56f_{n5,n6} = -\frac{2}{\tau_{y5}} \cdot \frac{\lambda_{n5}}{\lambda_{n6}} \cdot csch\left(\lambda_{n6} \cdot \tau_{x6}\right) \cdot F_{ss}\left(\lambda 6_{n6}, \lambda 5_{n5}, y_2, y_2, y_2, \tau_{y5}\right), \tag{C.13e}$$

$$ES56_{n5} = -\mu_6 \cdot \frac{\lambda_{n5}}{\tau_{y5}} \cdot J_{z6} \cdot F_{l2s}\left(\lambda 5_{n5}, y_2, y_2, \tau_{y5}\right). \tag{C.13f}$$

By using (32), the development of (26b) gives

$$f5^y_{n5} = -\left| \begin{array}{l} \sum_{h7=0}^{\infty} \left(c7^x_{h7} \cdot Q57c_{n5,h7} + d7^x_{h7} \cdot Q57d_{n5,h7}\right) \\ \cdots + \sum_{n7=1}^{\infty} \left(e7^y_{n7} \cdot Q57e_{n5,n7} + f7^y_{n7} \cdot Q57f_{n5,n7}\right) \\ \cdots - ES57_{n5} \end{array} \right., \tag{C.14a}$$

$$Q57c_{n5,h7} = \frac{2}{\tau_{y5}} \cdot \lambda_{n5} \cdot \left\{ \begin{array}{ll} -\left[y_3 \cdot F_s\left(\lambda 5_{n5}, y_2, y_2, \tau_{y5}\right) - F_{ls}\left(\lambda 5_{n5}, y_2, y_2, \tau_{y5}\right)\right] & \text{for } h7 = 0 \\ \frac{1}{\beta_{h7}} \cdot csch\left(\beta_{h7} \cdot \tau_{y7}\right) \cdot F_{shs}\left(\beta 7_{h7}, \lambda 5_{n5}, y_3, y_2, y_2, \tau_{y5}\right) & \text{for } h7 \neq 0 \end{array} \right. \tag{C.14b}$$

Preprints (www.preprints.org) | NOT PEER-REVIEWED | Posted: 27 September 2016 doi:10.20944/preprints201609.0106.v1

$$Q57d_{n5,h7} = \frac{2}{\tau_{y5}} \cdot \lambda_{n5} \cdot \begin{cases} \left[y_2 \cdot F_s\left(\lambda 5_{n5}, y_2, y_2, \tau_{y5}\right) - F_{ls}\left(\lambda 5_{n5}, y_2, y_2, \tau_{y5}\right)\right] & \text{for } h7 = 0 \\ \frac{-1}{\beta_{h7}} \cdot csch\left(\beta_{h7} \cdot \tau_{y7}\right) \cdot F_{shs}\left(\beta 7_{h7}, \lambda 5_{n5}, y_2, y_2, y_2, \tau_{y5}\right) & \text{for } h7 \neq 0 \end{cases} \tag{C.14c}$$

$$Q57e_{n5,n7} = \frac{2}{\tau_{y5}} \cdot \frac{\lambda_{n5}}{\lambda_{n7}} \cdot csch\left(\lambda_{n7} \cdot \tau_{x7}\right) \cdot F_{ss}\left(\lambda 7_{n7}, \lambda 5_{n5}, y_2, y_2, y_2, \tau_{y5}\right), \tag{C.14d}$$

$$Q57f_{n5,n7} = -\frac{2}{\tau_{y5}} \cdot \frac{\lambda_{n5}}{\lambda_{n7}} \cdot \coth\left(\lambda_{n7} \cdot \tau_{x7}\right) \cdot F_{ss}\left(\lambda 7_{n7}, \lambda 5_{n5}, y_2, y_2, y_2, \tau_{y5}\right), \tag{C.14e}$$

$$ES57_{n5} = -\mu_7 \cdot \frac{\lambda_{n5}}{\tau_{y5}} \cdot J_{z7} \cdot F_{l2s}\left(\lambda 5_{n5}, y_2, y_2, \tau_{y5}\right). \tag{C.14f}$$

Appendix C.7 Expression of $c6_0^x$, $d6_0^x$, $c6_{h6}^x$, $d6_{h6}^x$, $e6_{n6}^y$ and $f6_{n6}^y$ for Region 6

By using (4) and (27d), the development of (30a) and (30b) gives

$$c6_0^x = ES61_0 - \sum_{h1=1}^{\infty} d1_{h1}^x \cdot Q61d_{0,h1}, \tag{C.15a}$$

$$Q61d_{0,h1} = -\frac{1}{\tau_{y6}} \cdot \frac{1}{\tau_{x6}} \cdot \frac{1}{\beta_{h1}} \cdot th\left(\beta_{h1} \cdot \tau_{y1}\right) \cdot F_s\left(\beta 1_{h1}, x_1, x_2, \tau_{x6}\right), \tag{C.15b}$$

$$ES61_0 = \frac{1}{2} \cdot \frac{1}{\tau_{y6}} \cdot \mu_6 \cdot J_{z6} \cdot y_2^2. \tag{C.15c}$$

$$c6_{h6}^x = -\sum_{h1=1}^{\infty} d1_{h1}^x \cdot Q61d_{h6,h1}, \tag{C.16a}$$

$$Q61d_{h6,h1} = -\frac{2}{\tau_{x6}} \cdot \frac{\beta_{h6}}{\beta_{h1}} \cdot th\left(\beta_{h1} \cdot \tau_{y1}\right) \cdot F_{cs}\left(\beta 6_{h6}, \beta 1_{h1}, x_2, x_1, x_2, \tau_{x6}\right). \tag{C.16b}$$

By using (8) and (27d), the development of (30c) and (30d) gives

$$d6_0^x = ES62_0 - \sum_{h2=1}^{\infty} c2_{h2}^x \cdot Q62c_{0,h2}, \tag{C.17a}$$

$$Q62c_{0,h2} = \frac{1}{\tau_{y6}} \cdot \frac{1}{\tau_{x6}} \cdot \frac{1}{\beta_{h2}} \cdot th\left(\beta_{h2} \cdot \tau_{y2}\right) \cdot F_s\left(\beta 2_{h2}, x_1, x_2, \tau_{x6}\right), \tag{C.17b}$$

$$ES62_0 = \frac{1}{2} \cdot \frac{1}{\tau_{y6}} \cdot \mu_6 \cdot J_{z6} \cdot y_3^2. \tag{C.17c}$$

$$d6_{h6}^x = -\sum_{h2=1}^{\infty} c2_{h2}^x \cdot Q62c_{h6,h2}, \tag{C.18a}$$

$$Q62c_{h6,h2} = \frac{2}{\tau_{x6}} \cdot \frac{\beta_{h6}}{\beta_{h2}} \cdot th\left(\beta_{h2} \cdot \tau_{y2}\right) \cdot F_{cs}\left(\beta 6_{h6}, \beta 2_{h2}, x_2, x_1, x_2, \tau_{x6}\right). \tag{C.18b}$$

By using (24), the development of (31a) gives

$$e6_{n6}^y = -\left[\begin{array}{l} \sum_{h5=1}^{\infty}\left(c5_{h5}^x \cdot Q65c_{n6,h5} + d5_{h5}^x \cdot Q65d_{n6,h5}\right) \\ \cdots + \sum_{n5=1}^{\infty}\left(e5_{n5}^y \cdot Q65e_{n6,n5} + f5_{n5}^y \cdot Q65f_{n6,n5}\right) \end{array}\right] \tag{C.19a}$$

$$Q65c_{n6,h5} = -\frac{2}{\tau_{y6}} \cdot \frac{\mu_6}{\mu_5} \cdot csch\left(\beta_{h5} \cdot \tau_{y5}\right) \cdot F_{shs}\left(\beta 5_{h5}, \lambda 6_{n6}, y_3, y_2, y_2, \tau_{y6}\right), \tag{C.19b}$$

Preprints (www.preprints.org) | NOT PEER-REVIEWED | Posted: 27 September 2016 doi:10.20944/preprints201609.0106.v1

$$Q65d_{n6,h5} = \frac{2}{\tau_{y6}} \cdot \frac{\mu_6}{\mu_5} \cdot csch\left(\beta_{h5} \cdot \tau_{y5}\right) \cdot F_{shs}\left(\beta 5_{h5}, \lambda 6_{n6}, y_2, y_2, y_2, \tau_{y6}\right), \tag{C.19c}$$

$$Q65e_{n6,n5} = -\frac{2}{\tau_{y6}} \cdot \frac{\mu_6}{\mu_5} \cdot \coth\left(\lambda_{n5} \cdot \tau_{x5}\right) \cdot F_{ss}\left(\lambda 5_{n5}, \lambda 6_{n6}, y_2, y_2, y_2, \tau_{y6}\right), \tag{C.19d}$$

$$Q65f_{n6,n5} = \frac{2}{\tau_{y6}} \cdot \frac{\mu_6}{\mu_5} \cdot csch\left(\lambda_{n5} \cdot \tau_{x5}\right) \cdot F_{ss}\left(\lambda 5_{n5}, \lambda 6_{n6}, y_2, y_2, y_2, \tau_{y6}\right). \tag{C.19e}$$

By using (14), the development of (31b) gives

$$f6^{y}_{n6} = -\left[\sum_{h3=1}^{\infty}\left(c3^{x}_{h3} \cdot Q63c_{n6,h3} + d3^{x}_{h3} \cdot Q63d_{n6,h3}\right) + \sum_{n3=1}^{\infty} f3^{y}_{n3} \cdot Q63f_{n6,n3}\right], \tag{C.20a}$$

$$Q63c_{n6,h3} = -\frac{2}{\tau_{y6}} \cdot \frac{\mu_6}{\mu_3} \cdot \frac{\cos\left(\beta_{h3} \cdot \tau_{x3}\right)}{\mathrm{sh}\left(\beta_{h3} \cdot \tau_{y3}\right)} \cdot F_{shs}\left(\beta 3_{h3}, \lambda 6_{n6}, y_3, y_2, y_2, \tau_{y6}\right), \tag{C.20b}$$

$$Q63d_{n6,h3} = \frac{2}{\tau_{y6}} \cdot \frac{\mu_6}{\mu_3} \cdot \frac{\cos\left(\beta_{h3} \cdot \tau_{x3}\right)}{\mathrm{sh}\left(\beta_{h3} \cdot \tau_{y3}\right)} \cdot F_{shs}\left(\beta 3_{h3}, \lambda 6_{n6}, y_2, y_2, y_2, \tau_{y6}\right), \tag{C.20c}$$

$$Q63f_{n6,n3} = \frac{2}{\tau_{y6}} \cdot \frac{\mu_6}{\mu_3} \cdot \coth\left(\lambda_{n3} \cdot \tau_{x3}\right) \cdot F_{ss}\left(\lambda 3_{n3}, \lambda 6_{n6}, y_2, y_2, y_2, \tau_{y6}\right). \tag{C.20d}$$

Appendix C.8 Expression of $c7^{x}_{0}$, $d7^{x}_{0}$, $c7^{x}_{h7}$, $d7^{x}_{h7}$, $e7^{y}_{n7}$ and $f7^{y}_{n7}$ for Region 7

By using (4) and (32d), the development of (35a) and (35b) gives

$$c7^{x}_{0} = ES71_0 - \sum_{h1=1}^{\infty} d1^{x}_{h1} \cdot Q71d_{0,h1}, \tag{C.21a}$$

$$Q71d_{0,h1} = -\frac{1}{\tau_{y7}} \cdot \frac{1}{\tau_{x7}} \cdot \frac{1}{\beta_{h1}} \cdot th\left(\beta_{h1} \cdot \tau_{y1}\right) \cdot F_s\left(\beta 1_{h1}, x_1, x_4, \tau_{x7}\right), \tag{C.21b}$$

$$ES71_0 = \frac{1}{2} \cdot \frac{1}{\tau_{y7}} \cdot \mu_7 \cdot J_{z7} \cdot y_2^2. \tag{C.21c}$$

$$c7^{x}_{h7} = -\sum_{h1=1}^{\infty} d1^{x}_{h1} \cdot Q71d_{h7,h1}, \tag{C.22a}$$

$$Q71d_{h7,h1} = -\frac{2}{\tau_{x7}} \cdot \frac{\beta_{h7}}{\beta_{h1}} \cdot th\left(\beta_{h1} \cdot \tau_{y1}\right) \cdot F_{cs}\left(\beta 7_{h7}, \beta 1_{h1}, x_4, x_1, x_4, \tau_{x7}\right). \tag{C.22b}$$

By using (8) and (32d), the development of (35c) and (35d) gives

$$d7^{x}_{0} = ES72_0 - \sum_{h2=1}^{\infty} c2^{x}_{h2} \cdot Q72c_{0,h2}, \tag{C.23a}$$

$$Q72c_{0,h2} = \frac{1}{\tau_{y7}} \cdot \frac{1}{\tau_{x7}} \cdot \frac{1}{\beta_{h2}} \cdot th\left(\beta_{h2} \cdot \tau_{y2}\right) \cdot F_s\left(\beta 2_{h2}, x_1, x_4, \tau_{x7}\right), \tag{C.23b}$$

$$ES72_0 = \frac{1}{2} \cdot \frac{1}{\tau_{y7}} \cdot \mu_7 \cdot J_{z7} \cdot y_3^2. \tag{C.23c}$$

$$d7^{x}_{h7} = -\sum_{h2=1}^{\infty} c2^{x}_{h2} \cdot Q72c_{h7,h2}, \tag{C.24a}$$

$$Q72c_{h7,h2} = \frac{2}{\tau_{x7}} \cdot \frac{\beta_{h7}}{\beta_{h2}} \cdot th\left(\beta_{h2} \cdot \tau_{y2}\right) \cdot F_{cs}\left(\beta 7_{h7}, \beta 2_{h2}, x_4, x_1, x_4, \tau_{x7}\right). \tag{C.24b}$$

By using (24), the development of (36a) gives

$$f7^{y}_{n7} = -\left[\begin{array}{l}\sum\limits_{h5=1}^{\infty}\left(c5^{x}_{h5}\cdot Q75c_{n7,h5} + d5^{x}_{h5}\cdot Q75d_{n7,h5}\right)\\ \cdots + \sum\limits_{n5=1}^{\infty}\left(e5^{y}_{n5}\cdot Q75e_{n7,n5} + f5^{y}_{n5}\cdot Q75f_{n7,n5}\right)\end{array}\right], \tag{C.25a}$$

$$Q75c_{n7,h5} = -\frac{2}{\tau_{y7}}\cdot\frac{\mu_7}{\mu_5}\cdot\frac{\cos\left(\beta_{h5}\cdot\tau_{x5}\right)}{\mathrm{sh}\left(\beta_{h5}\cdot\tau_{y5}\right)}\cdot F_{shs}\left(\beta5_{h5},\lambda7_{n7},y_3,y_2,y_2,\tau_{y7}\right), \tag{C.25b}$$

$$Q75d_{n7,h5} = \frac{2}{\tau_{y7}}\cdot\frac{\mu_7}{\mu_5}\cdot\frac{\cos\left(\beta_{h5}\cdot\tau_{x5}\right)}{\mathrm{sh}\left(\beta_{h5}\cdot\tau_{y5}\right)}\cdot F_{shs}\left(\beta5_{h5},\lambda7_{n7},y_2,y_2,y_2,\tau_{y7}\right), \tag{C.25c}$$

$$Q75e_{n7,n5} = -\frac{2}{\tau_{y7}}\cdot\frac{\mu_7}{\mu_5}\cdot csch\left(\lambda_{n5}\cdot\tau_{x5}\right)\cdot F_{ss}\left(\lambda5_{n5},\lambda7_{n7},y_2,y_2,y_2,\tau_{y7}\right), \tag{C.25d}$$

$$Q75f_{n7,n5} = \frac{2}{\tau_{y7}}\cdot\frac{\mu_7}{\mu_5}\cdot\coth\left(\lambda_{n5}\cdot\tau_{x5}\right)\cdot F_{ss}\left(\lambda5_{n5},\lambda7_{n7},y_2,y_2,y_2,\tau_{y7}\right). \tag{C.25e}$$

By using (19), the development of (36b) gives

$$e7^{y}_{n7} = -\left[\sum_{h4=1}^{\infty}\left(c4^{x}_{h4}\cdot Q74c_{n7,h4} + d4^{x}_{h4}\cdot Q74d_{n7,h4}\right) + \sum_{n4=1}^{\infty} e4^{y}_{n4}\cdot Q74e_{n7,n4}\right], \tag{C.26a}$$

$$Q74c_{n7,h4} = -\frac{2}{\tau_{y7}}\cdot\frac{\mu_7}{\mu_4}\cdot csch\left(\beta_{h4}\cdot\tau_{y4}\right)\cdot F_{shs}\left(\beta4_{h4},\lambda7_{n7},y_3,y_2,y_2,\tau_{y7}\right), \tag{C.26b}$$

$$Q74d_{n7,h4} = \frac{2}{\tau_{y7}}\cdot\frac{\mu_7}{\mu_4}\cdot csch\left(\beta_{h4}\cdot\tau_{y4}\right)\cdot F_{shs}\left(\beta4_{h4},\lambda7_{n7},y_2,y_2,y_2,\tau_{y7}\right), \tag{C.26c}$$

$$Q74e_{n7,n4} = -\frac{2}{\tau_{y7}}\cdot\frac{\mu_7}{\mu_4}\cdot\coth\left(\lambda_{n4}\cdot\tau_{x4}\right)\cdot F_{ss}\left(\lambda4_{n4},\lambda7_{n7},y_2,y_2,y_2,\tau_{y7}\right). \tag{C.26d}$$

References

1. Yilmaz, M.; Krein, P.T. Capabilities of finite element analysis and magnetic equivalent circuits for electrical machine analysis and design. In Proc. PESC, Rhodes, Greece, June 15-19, 2008.
2. Dubas, F.; Espanet, C. Analytical solution of the magnetic field in permanent-magnet motors taking into account slotting effect: No-load vector potential and flux density calculation. *IEEE Trans. on Magn.* **2009**, *45*, 2097-2109.
3. Zhu, Z.Q.; Wu, L.J.; Xia, Z.P. An accurate subdomain model for magnetic field computation in slotted surface-mounted permanent-magnet machines. *IEEE Trans. on Magn.* **2010**, *46*, 1100-1115.
4. Rahideh, A.; Korakianitis, T. Analytical calculation of open-circuit magnetic field distribution of slotless brushless PM machines. *Electrical Power and Energy Systems* **2012**, *44*, 99-114.
5. Tiegna, H.; Amara, Y.; Barakat, G. Overview of analytical models of permanent magnet electrical machines for analysis and design purposes. *Mathematics and Computer in Simulation* **2013**, *90*, 162-177.
6. Curti, M.; Paulides, J.J.H.; Lomonova, E.A. An overview of analytical methods for magnetic field computation. In Proc. EVER, Grimaldi Forum, Monaco, March 31-April 02, 2015.
7. Lehmann, T. Méthode graphique pour déterminer le trajet des lignes de force dans l'air. *Revue d'Électricité: La Lumière Électrique* **1909**, *43-45*, 103-110 & 137-142 & 163-168.
8. Flux2D, General operating instructions – Version 10.2.1. Cedrat S.A. Electrical Engineering, 2008, Grenoble, France.
9. Jin, J. *The finite element method in electromagnetic – Second Edition*, New York: John Wiley & Sons, Inc., 2002.
10. Stoll, R.L. *The analysis of eddy currents*, Clarendon press – Oxford, 1974.
11. Smith, G.D. *Numerical solution of partial differential equations: Finite difference methods – Third edition*, Clarendon press – Oxford, 1985.

12. Wrobel, L.C.; Aliabadi, M.H. *The boundary element method*, New York: John Wiley & Sons, Inc., 2002.
13. Alger, P.L. *Induction machines: Their behavior and uses*, Gordon and Breach Publisher, 1970.
14. Holman, J.P. *Heat transfer – Sixth edition*, McGraw-Hill Book Compagny, 1986.
15. Roters, H.C. *Electromagnetic devices*, New York: John Wiley & Sons, Inc., 1941.
16. Ostovic, V. *Dynamics of saturated electric machines*, New York: Springer-Verlag, 1989.
17. Driscoll, T.A.; Trefethen, L.N. *Schwarz-Christoffel mapping*, Cambridge, U.K.: Cambridge Univ. Press, 2002.
18. Sylvester, P. *Modern electromagnetic fields*, London, U.K.: Prentice-Hall, 1968.
19. Binns, K.J.; Lawrenson, P.J.; Trowbridge, C.W. *The analytical and numerical solution of electric and magnetic fields*, New York: John Wiley & Sons, Inc., 1992.
20. Hague, B. *Electromagnetic problems in electrical engineering*, London, U.K.: Oxford Univ. Press, 1929.
21. Melcher, J.R. *Continuum electromechanics*, Cambridge, MA: MIT Press, 1981.
22. Farlow, S.J. *Partial differential equations for scientists and engineers*, New York: Dover, Inc., 1993.
23. Schutte, J.; Strauss, J.M. Optimisation of a transverse flux linear PM generator using 3D Finite Element Analysis. In Proc. ICEM, Rome, Italy, Sept. 06-08, 2010.
24. Espanet, C.; Kieffer, C.; Mira, A.; Giurgea, S.; Gustin, F. Optimal design of a special permanent magnet synchronous machine for magnetocaloric refrigeration. In Proc. ECCE, Denver, Colorado, USA, Sept. 15-19, 2013.
25. Ede, J.D.; Atallah, K.; Jewel, G.W.; Wang, J.B.; Howe, D. Effect of axial segmentation of permanent magnets on rotor loss in modular permanent-magnet brushless machines. *IEEE Trans. on Ind. Appl.* **2007**, *43*, 1207-1213.
26. Vansompel, H.; Sergeant, P.; Dupré, L. A multilayer 2-D – 2-D coupled model for eddy current calculation in the rotor of an axial-flux PM machine. *IEEE Trans. on Energy Conv.* **2012**, *27*, 784-791.
27. Benlamine, R.; Dubas, F.; Randi, S-A.; Lhotellier, D.; Espanet, C. 3-D numerical hybrid method for PM eddy-current losses calculation: Application to axial-flux PMSMs. *IEEE Trans. on Magn.* **2015**, *51*, Art. ID 8106110.
28. Carter, F.W. Air-gap induction. *Electrical World and Engineer* **1901**, *XXXVIII*, 884-888.
29. Kumar, P.; Bauer, P. Improved analytical model of a permanent-magnet brushless DC motor. *IEEE Trans. on Magn.* **2008**, *44*, 2299-2309.
30. Dalal, A.; Kumar, P. Analytical model of a permanent magnet Brushless DC Motor with non-linear ferromagnetic material. In Proc. ICEM, Berlin, Germany, Sept. 02-05, 2014.
31. Dalal, A.; Kumar, P. Analytical model for permanent magnet motor with slotting effect, armature reaction, and ferromagnetic material property. *IEEE Trans. on Magn.* **2015**, *51*, Art. ID 8114910.
32. Boules, N. Two-dimensional field analysis of cylindrical machines with permanent magnet excitation. *IEEE Trans. on Ind. Appl.* **1984**, *IA-20*, 1267-1277.
33. Moallem, M.; Madhkhan, M. Predicting the parameters and performance of brushless DC motor including saturation and slotting effects and magnetic circuit variations. In Proc. PEDS, Univ. of Singapore, Singapore, Feb. 21-24, 1995.
34. Abbaszadeh, K.; Alam, F.R. On-load field component separation in surface-mounted permanent magnet motors using an improved conformal mapping method. *IEEE Trans. on Magn.* **2016**, *52*, Art. ID 5200112.
35. Berkani, M.S.; Sough, M.L.; Giurgea, S.; Dubas, F.; Boualem, B.; Espanet, C. A simple analytical approach to model saturation in surface mounted permanent magnet synchronous motors. In Proc. ECCE, Montreal, Canada, Sept. 20-24, 2015.
36. Mishkin, E. Theory of the squirrel-cage induction machine derived directly from Maxwell's field equations. *Quart. Journ. Mech. and Applied Math.* **1954**, *7*, 472-487.
37. Cullen, A.L.; Barton, T.H. A simplified electromagnetic theory of the induction motor, using the concept of wave impedance. *Proc. IEE* **1958**, *105C*, 331-336.
38. Greig, J.; Freeman, E.M. Travelling-wave problem in electrical machines. *Proc. IEE* **1967**, *114*, 1681–1683.
39. Freeman, E.M. Travelling waves in induction machines: input impedance and equivalent circuits. *Proc. IEE* **1968**, *115*, 1772-1776.
40. Jones, C.V.; Gibson, R.C. Correlation of the air-gap vector potential of an induction motor with the magnetising current. *Proc. IEE*, (116), 3, 1969, pp. 385-390.
41. Williamson, S. The anisotropic layer theory of induction machines and induction devices. *J. Inst. Maths Applics* **1967**, *17*, 69-84.

42. Gieras, J. Analysis of multilayer rotor induction motor with higher space harmonics taken into account. *Proc. IEE* **1991**, *138*, 59-67.
43. Panaitescu, A.; Panaitescu, I. A field model for induction machines. In Proc. ICEM, Vigo, Spain, Sept. 10-12, 1996.
44. Madescu, G.; Boldea, I.; Miller, T.J.E. An analytical iterative model (AIM) for induction motor design. In Proc. IEEE IAS Annual Meeting, San Diego, CA, Oct. 06-10, 1996.
45. Sprangers, R.L.J.; Motoasca, T.E.; Lomonova, E.A. Extended anisotropic layer theory for electrical machines. *IEEE Trans. on Magn.* **2013**, *49*, 2217-2220.
46. Sprangers, R.L.J.; Paulides, J.J.H.; Boynov, K.O.; Lomonova, E.A.; Waarma, J. Comparison of two anisotropic layer models applied to induction motors. *IEEE Trans. on Ind. Appl.* **2014**, *50*, 2533-2543.
47. Sprangers, R.L.J.; Paulides, J.J.H.; Gysen, B.L.J.; Lomonova, E.A. Magnetic saturation in semi-analytical harmonic modeling for electric machine analysis. *IEEE Trans. on Magn.* **2016**, *52*, Art. ID 8100410.
48. Djelloul, K.Z.; Boughrara, K.; Ibtiouen, R.; Dubas, F. Nonlinear analytical calculation of magnetic field and torque of switched reluctance machines. In Proc. CISTEM, Marrakech-Benguérir, Maroc, Oct. 26-28, 2016.
49. Sprangers, R.L.J.; Paulides, J.J.H.; Gysen, B.L.J.; Waarma, J.; Lomonova, E.A. Semi-analytical framework for synchronous reluctance motor analysis including finite soft-magnetic material permeability. *IEEE Trans. on Magn.* **2015**, *5*, Art. ID 81105204.
50. Abdel-Razek, A.A.; Coulomb, J.L.; Feliachi, M.; Sabonnadière, J.C. The calculation of electromagnetic torque in saturated electric machines within combined numerical and analytical solutions of the field equations. *IEEE Trans. on Magn.* **1981**, *17*, 3250–3252.
51. Féliachi, M.; Coulomb, J.L.; Mansir, H. Second order air-gap element for the dynamic finite-element analysis of the electromagnetic field in electric machines. *IEEE Trans. on Magn.* **1983**, *19*, 2300–2303.
52. Goby, F.; Razek, A. Numerical calculation of electromagnetic forces. *Mathematics and Computer in Simulation* **1987**, *29*, 343–350.
53. Liu, Z.J.; Bi, C.; Tan, H.C.; Low, T.S. A combined numerical and analytical approach for magnetic field analysis of permanent magnet machines. *IEEE Trans. on Magn.* **1995**, *31*, 1372–1375.
54. Mirzayee, M.; Mehrjerdi, H.; Tsurkerman, I. Analysis of a high-speed solid rotor induction motor using coupled analytical method and reluctance networks. In Proc. ACES, Honolulu, Hawaii, April 03-07, 2005.
55. Gholizad, H.; Mirsalim, M.; Mirzayee, M. Dynamic Analysis of Highly Saturated Switched Reluctance Motors Using Coupled Magnetic Equivalent Circuit and the Analytical Solution. In Proc. CEM, Miami, Florida, USA, April 04-07, 2006.
56. Mirzayee, M.; Mirsalim, M.; Gholizad, H.; Arani, S.J. Combined 3D Numerical and Analytical Computation Approach for Analysis and Design of High Speed Solid Iron rotor Induction Machines. In Proc. CEM, Aachen, Germany, April 04-06, 2006.
57. Ghoizad, H.; Mirsalim, M.; Mirzayee, M.; Cheng, W. Coupled magnetic equivalent circuits and the analytical solution in the air-gap of squirrel cage induction machines. *Int. Journal of Applied Electromagnetics and Mechanics* **2007**, *25*, 749-754.
58. Hemeida, A.; Sergeant, P. Analytical modeling of surface PMSM using a combined solution of Maxwell's equations and magnetic equivalent circuit. *IEEE Trans. on Magn.* **2014**, *50*, Art. ID 7027913.
59. Laoubi, Y.; Dhifli, M.; Verez, G.; Amara, Y.; Barakat, G. Open circuit performance analysis of a permanent magnet linear machine using a new hybrid analytical model. *IEEE Trans. on Magn.* **2015**, *51*, Art. ID 8102304.
60. Ouagued, S.; Diriyé, A.A.; Amara, Y.; Barakat, G. A General Framework Based on a Hybrid Analytical Model for the Analysis and Design of Permanent Magnet Machines. *IEEE Trans. on Magn.* **2015**, *51*, Art. ID 8110204.
61. Pluk, K.J.W.; Jansen, J.W.; Lomonova, E.A. Hybrid analytical modeling: Fourier modeling combined with mesh-based magnetic equivalent circuits. *IEEE Trans. on Magn.* **2015**, *51*, Art. ID 8106812.
62. Pluk, K.J.W.; Jansen, J.W.; Lomonova, E.A. 3-D hybrid analytical modeling: 3-D Fourier modeling combined with mesh-based 3-D magnetic equivalent circuits. *IEEE Trans. on Magn.* **2015**, *51*, Art. ID 8208614.
63. Zhang, Z.; Xia, C.L.; Yan, Y.; Wang, H.M. Analytical field calculation of doubly fed induction generator with core saturation considered. In Proc. PEMD, Glasgow, UK, 19-21 April, 2016.
64. Dubas, F. Conception d'un moteur rapide à aimants permanents pour l'entraînement de compresseurs de piles à combustible. Ph.D. dissertation, Electrical Engineering and Systems (LEES), University of Franche-Comté (UFC), Belfort, France, 2006.

65. Dubas, F.; Rahideh, A. 2-D analytical PM eddy-current loss calculations in slotless PMSM equipped with surface-inset magnets. *IEEE Trans. on Magn.* **2014**, *50*, Art. ID 6300320.